



**HAL**  
open science

# Homogenization of Geostationary Infrared Imager Channels for Cold Cloud Studies Using Megha-Tropiques/ScaRaB

Thomas Fiolleau, Rémy Roca, Sophie Cloché, Dominique Bouniol, Patrick Raberanto

► **To cite this version:**

Thomas Fiolleau, Rémy Roca, Sophie Cloché, Dominique Bouniol, Patrick Raberanto. Homogenization of Geostationary Infrared Imager Channels for Cold Cloud Studies Using Megha-Tropiques/ScaRaB. IEEE Transactions on Geoscience and Remote Sensing, 2020, 58, pp.6609 - 6622. 10.1109/tgrs.2020.2978171 . hal-03000650

**HAL Id: hal-03000650**

**<https://cnrs.hal.science/hal-03000650v1>**

Submitted on 12 Nov 2020

**HAL** is a multi-disciplinary open access archive for the deposit and dissemination of scientific research documents, whether they are published or not. The documents may come from teaching and research institutions in France or abroad, or from public or private research centers.

L'archive ouverte pluridisciplinaire **HAL**, est destinée au dépôt et à la diffusion de documents scientifiques de niveau recherche, publiés ou non, émanant des établissements d'enseignement et de recherche français ou étrangers, des laboratoires publics ou privés.

## AUTHOR QUERIES

### AUTHOR PLEASE ANSWER ALL QUERIES

**PLEASE NOTE:** We cannot accept new source files as corrections for your article. If possible, please annotate the PDF proof we have sent you with your corrections and upload it via the Author Gateway. Alternatively, you may send us your corrections in list format. You may also upload revised graphics via the Author Gateway.

- 1) Please be aware that authors are required to pay overlength page charges (\$230 per page) if the article is longer than 6 pages. If you cannot pay any or all of these charges please let us know. GRS Society members receive a discounted rate of \$200 per page.
- 2) This pdf contains 2 proofs. The first half is the version that will appear on Xplore. The second half is the version that will appear in print. If you have any figures to print in color, they will be in color in both proofs.
- 3) The “Open Access” option for your article expires when the article is published on Xplore in an issue with page numbers. Articles in “Early Access” may be changed to Open Access. If you have not completed your electronic copyright form (ECF) and payment option please return to Scholar One “Transfer Center.” In the Transfer Center you will click on “Manuscripts with Decisions” link. You will see your article details and under the “Actions” column click “Transfer Copyright.” From the ECF it will direct you to the payment portal to select your payment options and then return to ECF for copyright submission.

AQ:1 = Please note that “viewing zenithal angle” has been changed to “viewing zenith angle” throughout the text for consistency.

AQ:2 = Please confirm or add details for any funding or financial support for the research of this article.

AQ:3 = Please confirm whether the edits made in the current affiliation of all the authors are correct.

AQ:4 = Please confirm the postal code for CNRS, Institut Pierre Simon Laplace, Université de Toulouse, and Laboratoire de Météorologie Dynamique.

AQ:5 = Please provide the expansions for SEVIRI and AMSU.

AQ:6 = Please check the sentence “The use of geophysical targets like ...” for clarity.

AQ:7 = Please check and confirm whether the edits made are appropriate: “Some studies on these geometric effects discussed the different configurations of cloud fields.”

AQ:8 = Please provide the organization name, organization location, and report no. for Refs. [11] and [12].

AQ:9 = Please provide the organization location and report no. for Ref. [19].

AQ:10 = Please provide the volume no. for Ref. [25].

AQ:11 = Please provide the organization name and organization location for Refs. [30] and [31].

AQ:12 = Please provide the year of completion when the author Rémy Roca received the M.S. degree.

AQ:13 = Please provide the year of completion when the author Sophie Cloché received the M.S. degree.

AQ:14 = Please provide the location for CETP.

# Homogenization of Geostationary Infrared Imager Channels for Cold Cloud Studies Using Megha-Tropiques/ScaRaB

Thomas Fiolleau<sup>ID</sup>, Rémy Roca, Sophie Cloché, Dominique Bouniol, and Patrick Raberanto

**Abstract**—Infrared (IR) observations from the fleet of multi-agencies meteorological geostationary satellites have a great potential to support scientific and operational investigations at a quasi-global scale. In particular, such a data record, defined as the GEOring data set, is well suited to document the tropical convective systems life cycles by applying cloud tracking algorithms. Yet, this GEOring data set is far from being homogeneous, preventing the realization of its potential. A number of sources of inhomogeneities are identified ranging from spatiotemporal resolutions to spectral characteristics of the IR channels and calibration methodologies. While previous efforts have attempted to correct such issues, the adjustment of the cold part of the IR spectrum remains unfit for cold cloud studies. Here, a processing method is introduced to minimize the inhomogeneities against a reference observational data set from the Scanner for Radiation Budget (ScaRaB) instrument onboard the Megha-Tropiques satellite. The method relies on the collocations between the geostationary observations and the reference. The techniques exhibit significant sensitivity to the selection of the relevant pairs of observations requiring a dedicated filtering of the data. A second effort is then proposed to account for the limb-darkening effect and a method is developed to correct the brightness temperature (BT) dependence on the geostationary viewing zenith angle (VZA). Overall, results show a residual after the processing of 0 K between any of the geostationary data and the ScaRaB reference. The final calibrated and limb-adjusted IR observations are then homogeneous for cold BT lower than 240 K with a standard deviation lower than 1.5 K throughout the GEOring.

**Index Terms**—Calibration and spectral corrections, cold cloud studies, geostationary satellites, infrared (IR) image sensors, limb-darkening corrections.

## I. INTRODUCTION

METEOROLOGY agencies monitor individually operational geostationary platforms, which when used all together permit an observation for all longitudes of the Earth

Manuscript received July 17, 2019; revised November 25, 2019 and January 22, 2020; accepted February 4, 2020. (*Corresponding author: Thomas Fiolleau.*)

Thomas Fiolleau and Rémy Roca are with the Laboratoire d'Etudes en Géophysique et Océanographie Spatiales, CNRS, 31400 Toulouse, France (e-mail: thomas.fiolleau@legos.obs-mip.fr; remy.roca@legos.obs-mip.fr).

Sophie Cloché is with CNRS, Institut Pierre Simon Laplace, 75252 Paris, France (e-mail: sophie.bouffies-cloche@ipsl.fr).

Dominique Bouniol is with the Centre National de Recherches Météorologiques, CNRS, Météo-France, Université de Toulouse, 31057 Toulouse, France (e-mail: dominique.bouniol@meteo.fr).

Patrick Raberanto is with the Laboratoire de Météorologie Dynamique, CNRS, 75016 Paris, France (e-mail: patrick.raberanto@lmd.polytechnique.fr).

Color versions of one or more of the figures in this article are available online at <http://ieeexplore.ieee.org>.

Digital Object Identifier 10.1109/TGRS.2020.2978171

on a large latitudinal band ( $\sim 60^\circ$  S– $60^\circ$  N) with similar instruments. The potential benefit of such an observing capability has triggered numerous efforts in the past 40 years to make use of it for various applications, ranging from the elaboration of a unique perspective on clouds studies [1], [2] for precipitation estimation [3], climate studies [4], and global visualization applications [5]. Yet, when carefully examined, this GEOring appears to be far from a homogenous suite of instruments operated in a similar fashion. The space/time resolution and sampling differ across the platforms. The acquisition procedure also differs among the satellites (from South to North, North to South, or by sector). The calibration procedure of each instrument is also performed at the individual level with the instruments' specific modes of operation. Since 2011, for the infrared (IR) channels, the agencies provide alternative calibration coefficients obtained from a statistical comparison to hyperspectral IR measurements from low earth-orbiting satellites using the common methodology of the Global Space-Based InterCalibration System (GSICS) [6]. Nevertheless, the GSICS currently only provides calibration coefficients referenced to the NASA Earth Observing System (EOS), Aqua Atmospheric IR Sounder (AIRS), and the Exploitation of Meteorological Satellites (EUMETSAT)–Centre National d'Etudes Spatiales (CNES), Meteorological Operation (MetOp), and IR Atmospheric Sounding Interferometer (IASI) calibration standard. This harmonization effort does not take into account spectral band responses and viewing angle effects, which are needed for sensor homogenization. Indeed, while often referred to as a unique IR channel, the multiple instruments do show some spectral differences as well.

Most of the spectral imagers onboard geostationary satellites monitor with a relatively high temporal frequency the calibration coefficients for thermal IR channels by using onboard blackbody references. Some of the differences in the temperature measurements from one geostationary satellite to another can be explained by the differences in the calibration references, methods, as well as in the spectral filter functions. Moreover, it has been observed that the spectral imagers may degrade over time with different rates [7], [8]. The geostationary imagers can also be affected by short-term variations. The accumulation of ice on the surface of the imager optics modifies their spectral response function (SRF) and consequently affects the measurement of the temperatures. To face these issues, decontamination events are regularly applied to the radiometers inducing

TABLE I  
SUMMARY OF THE TECHNICAL CHARACTERISTICS OF THE VARIOUS EXISTING IR GEORING DATA SETS

Products	Spatial resolution	Temporal resolution	Spatial coverage	Temporal coverage	Calibration and temporal normalization	Limb darkening correction	Data source
Gridsat-B1	0.07°	180 min	70°S-70°N	1980-present	HIRS channel 8 [14]	Yes	ISCCP-B1
CPC	~ 0.04°	30 min	60°S-60°N	2000-present	No absolute calibration and no temporal normalization	Yes	Native
CLAUS	0.5°	180 min	Global*	1983-2006	ISCCP- B3	Yes	ISCCP-B3
CLAUS	0.3°	180 min	Global*	1985-2008	ISCCP- B3	Yes	ISCCP-B3
ISCCP-B1	Native FoV subsampled to ~ 0.1°	180 min	70°S-70°N	1980-present	AVHRR channel 5 [13]	No	Native
ISCCP-B3	Native FoV subsampled to ~ 0.3°	180 min	70°S-70°N	1983-2009	AVHRR channel 5 [13]	No	Native
This study	0.04°	30 min	35°S-35°N	2012-2016	SCARAB-IR channel 4	yes	Native

instability in the temperature measurements [9]. This effect has been particularly shown for the Meteosat Visible IR Imager (MVISIR) onboard the Meteosat-7 geostationary platform.

A diurnal cycle effect can also affect the imager calibration, especially for the instruments on the three-axis stabilized geostationary platforms [7], [9]. It has been shown that the sun-synchronous orbits of MetOp/IASI and EOS/AIRS used in the GSICS calibration are not sufficient to completely correct the diurnal IR calibration issues [10]. The precessing orbit of the tropical rainfall measuring mission (TRMM) platform and the observations of its visible and IR scanner (VIRS) have then been used to quantify and correct such a midnight IR calibration anomaly [10]. IR observations are also dependent on the geostationary viewing zenith angle (VZA). The issue is called limb darkening, corresponding to a decrease in the temperature as the VZA increases.

These multiple sources of inhomogeneity have prevented the full use of this unique observational capability, although a number of successful projects have attempted to overcome the above-listed limitations. Indeed, a number of significant efforts have been proposed in the last two decades to produce more or less homogeneous “global” archive of geostationary data sets for various applications. It ranges from cloud climatology computations (International Satellite Cloud Climatology Project (ISCCP)-B1, ISCCP-B3, and Cloud Archive User Service (CLAUS) [11]), hurricane trend analysis, support of precipitation estimation (Gridded Satellite (GridSat) [12]), real-time monitoring of precipitation (Climate Prediction Center (CPC) [13]), for the enhancement of radiation budget averages [8]. Additional information on these GEORing data sets is listed in [4]. Table I summarizes the available IR GEORing data sets altogether with their respective properties

and homogeneity levels. The ISCCP-B1 and B3 have been subsampled to a 180-min temporal resolution and to, respectively, ~0.1° and ~0.3° spatial resolution. They have been calibrated and spectrally normalized using advanced very high-resolution radiometer (AVHRR) observations [14]. The CLAUS data sets rely on the ISCCP-B3 and have been reprojected to an equal angle map projection with a spatial resolution of 0.3° and 0.5°. The GridSat-B1 is based on the ISCCP-B1 data set remapped to a 0.07° regular grid. In addition to the intercalibration used for the ISCCP data set, a second calibration using the high-resolution IR radiation sounder (HIRS) observations has been applied to correct a bias at cold temperatures observed after 2001. The CPC product is built in real time from native geostationary observations. The data are remapped to a regular grid of ~0.04° spatial resolution and are available every 30 min. To reduce the spectral differences and calibration issues, a complex, multistep, multiregional procedure is applied by comparing the brightness temperatures (BTs) from pairs of geostationary platforms. However, this procedure does not provide any absolute calibration. Also note that a limb correction has been performed on the GridSat-B1, CPC, and CLAUS data. In short, while a number of efforts have paved the way for a quantitative use of the GEORing data sets, no dedicated effort toward the cold BT regimes has been promoted so far. Yet, cold cloud studies benefit a lot from geostationary IR observations, for cloud microphysical or macrophysical parameters retrievals. The spatiotemporal resolution of the measurements further allows the life cycle analysis of the cold cloudiness and the estimation of related parameters. The present GEORing attempt is directed toward these scientific applications. In particular, it will serve as the input of the realization of a tropical mesoscale convective system data set using the TOOCAN algorithm [15].

TABLE II  
 TECHNICAL CHARACTERISTICS OF THE OPERATIONAL GEOSTATIONARY SATELLITES FLEET AND THE ASSOCIATED  
 IMAGERS USED OVER THE 2012–2016 PERIOD

Platform	Nadir location	Instrument	Central wavelength	Spectral interval	Spatial resolution at nadir	Temporal resolution	Region of interest	Source	Period
GOES-15	135° W	IMAGER	10.7 μm	10.2-11.2 μm	4 km	30 min	180° W-105° W 35° S-35° N	NOAA / DWD	Jan 2012- Dec 2016
GOES-13	75° W	IMAGER	10.7 μm	10.2-11.2 μm	4 km	30 min	111° W-30° W 35° S-35° N	NOAA / DWD	Jan 2012- Dec 2016
METEOSAT-8/9/10	0°	SEVIRI	10.8 μm	9.8-11.8 μm	3 km	15 min	45° W-45° E 35° S-35° N	EUMETSAT/ AERIS	Jan 2012- Dec 2016
METEOSAT-7 (IODC)	57.5° E	MVIRI	11.5 μm	10.5-12.5 μm	5 km	30 min	12° E-107° E 35° S-35° N	EUMETSAT/ AERIS	Jan 2012- Dec 2016
MTSAT-2	145° E	IMAGER	10.8 μm	10.3-11.3 μm	4 km	30 min	94° E-170° W 35° S-35° N	AERIS/ CIMSS	Jan 2012- May 2015
HIMAWARI-8	140.7° E	AHI	11.2 μm	11.0-11.4 μm	2 km	10 min	94° E-170° W 35° S-35° N	AERIS/ JMA	Jun 2015- Dec 2016

148 Such analyses require observations with a minimal temporal  
 149 resolution of 30 min [15], [16] to ensure tracked objects  
 150 overlap between two images. Such kind of studies requires the  
 151 use of thresholds applied to BT, ranging from 200 to 240 K,  
 152 depending upon the analysis [17], [15]. A homogeneous data  
 153 set is then mandatory, if one wants to proceed with the whole  
 154 tropical belt. The homogeneity and basic requirements for a  
 155 GEOring IR data set geared toward tropical cold cloud tracking  
 156 applications can be summarized as follows:

- 157 1) High-resolution spatial footprint and high spatial reso-  
 158 lution (~5 km).
- 159 2) A minimum of 30 min time sampling.
- 160 3) A spatial coverage dedicated to the tropics.
- 161 4) Homogenized BTs through spectral and calibration  
 162 adjustment.
- 163 5) Limb adjustment of IR observations.

164 Matching these requirements with the specifications of the  
 165 IR data sets summarized in Table I confirms the need for  
 166 a dedicated level 1c GEOring IR tailored for cold cloud  
 167 tracking applications. Moreover, the current implementation  
 168 of the GSICS coefficients computation is directed toward the  
 169 warm part of the spectrum [8], ruling out its use for cold  
 170 cloud studies calling for an alternative, cold cloud compliant,  
 171 absolute calibration reference for the GEOring. The limb  
 172 effect is less strong over the cold part of the temperature  
 173 spectrum than at the warm and clear sky end of the spectrum,  
 174 and the limb correction is easier to set up for cold cloudy  
 175 scenes (BTs < 240 K) than for the clear atmosphere. This

effect is strongly nonlinear and is thought to be impactful  
 only for the viewing angle above 26.5° [11]; it may still  
 require a correction for a homogeneous interpretation of the  
 BT field all through the image. It is difficult to establish  
 requirements once and for all in terms of residuals difference  
 in the homogeneous data, based on the radiometric noise of the  
 first generation sensors and the various sources of uncertainties  
 in the adjustment procedure and basic cloud-oriented retrievals  
 sensitivity. We propose to target a less than 1.5 K standard  
 deviation among any of the two geostationary satellites in the  
 final calibrated and limb-adjusted product for BTs < 240 K.

## II. DATA

### A. Five-Year Database of IR Geostationary Observations Over the Entire Tropics

Thermal channel BT images obtained by the operational  
 meteorological geostationary satellite fleet are used over  
 the 35°S–35°N latitude belt and for the whole 2012–2016  
 period. Table II shows the geostationary IR data used to  
 cover the entire tropics for this period. The geostationary  
 data set has been collected from different sources: the U.S.  
 National Oceanic and Atmospheric Administration (NOAA),  
 the European Organization for the Exploitation of Meteorological Satellites (EUMETSAT), the Japan Meteorological Agency (JMA), and the French Atmosphere and Service Data Pole (AERIS). Note that the Multifunctional Transport Satellite (MTSAT) data set has also been completed from the Space Science and Engineering Center (SSEC) of the University of

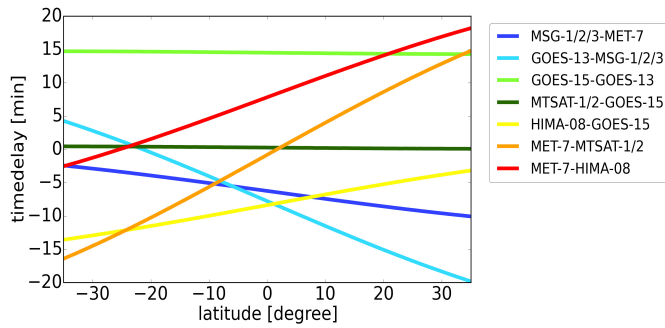


Fig. 1. Time delay of acquisition between pairs of geostationary images according to the latitude.

Wisconsin–Madison. The technical characteristics of each geostationary platform and their imagers are described in Table II and can differ from one platform to another. First, considering the temporal resolution, Meteorat Second Generation (MSG) and HIMAWARI-8 observe the Earth, respectively, with a 15- and 10-min time resolution, while the other platforms display a 30-min temporal resolution. Similarly, the scan-times vary from 7 min for HIMAWARI-8 to 25 min for Meteorat-7. The Geostationary Operational Environmental Satellite (GOES)-13 and GOES-15 sensors follow a complex scanning sector schedule. The full disk images are produced every 3 h, while the northern hemisphere and the southern hemisphere images are produced every 30 min with a time lag of few minutes between each scan. Also, note that the scanning schedule of MTSAT-2 does not provide half-hourly sampling of the southern hemisphere region. Contrary to the other imagers, the GOES-13 imager starts its earth scan at 15 and 45 min of the hour. Also note that Meteorat first- and second-generation imagers start their earth scan from the southeast corner, whereas NOAA and JMA platforms begin their earth scan from the northwest corner. All these temporal scanning differences imply some time delays between neighboring platforms observing the same region (Fig. 1). While the 15-min time delay is constant for the pairs of the GOES-15/GOES-13 and MTSAT-2/GOES-15 platforms, the time delay varies according to the latitude for the other pairs of geostationary platforms. At 35° S, a maximum time delay is found for the pair of MSG/GOES-13 platform of around 20 min. The maximum time delay amplitude accounted for the pair of the Meteorat-7/MTSAT-2 platforms and varies between -16 and 15 min.

Depending on the considered satellite, spatial resolution at nadir differs from one geostationary satellite to another and ranges from 2 km for HIMAWARI-8 to 5 km for Meteorat-7. In addition to the resolutions disparities, the GEOing is also characterized by differences in the central wavelength and the associated SRFs of each of the instruments (Fig. 2). While the central wavelength ranges between 10.7 and 11.5  $\mu\text{m}$  for the GOES imagers and the Meteorat-7 imager, respectively, two types of SRFs can define the IR channels. The GOES-13, GOES-15, MTSAT-2, and HIMAWARI-8 imagers display narrowband channels with a bandwidth lower than 1  $\mu\text{m}$ , whereas the Meteorat-7/MVIRI and MSG/SEVIRI imagers exhibit

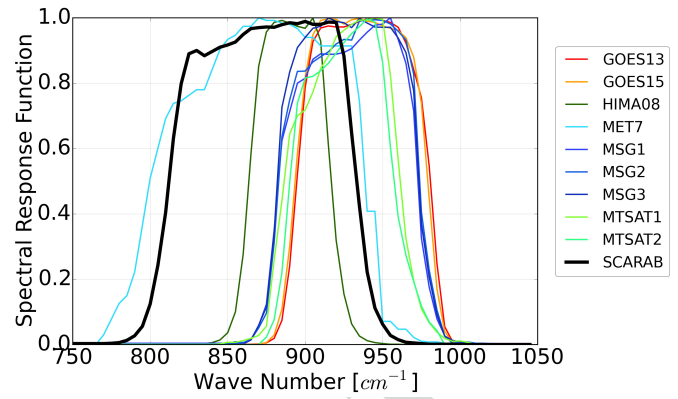


Fig. 2. SRF of the IR channel of the GEOing. The black line is the spectral response of the channel 4 of the ScaRaB instrument.

broader channels characterized by a 2  $\mu\text{m}$  bandwidth. A broadband channel is highly sensitive to ice contamination on the optics of the imagers, modifying their SRFs, and consequently, introducing a calibration error. Operational decontamination procedures are applied regularly to remove the ice build-up on the optics. Thus, spectral differences, as well as the individual satellite calibration procedures, contribute to the GEOing radiometric inhomogeneities.

### B. Megha-Tropiques/ScaRaB-3 Observations

The Scanner for Radiation Budget (ScaRaB) instrument on the Megha-Tropiques platform [18] is the third of its kind [19], [20] and has been designed to measure the Earth radiation components at the top of the atmosphere with high accuracy (<1%). The instrument acquires data across the satellite track with a swath of  $\sim 2200$  km from 30° S to 30° N. It is a broadband radiometer with four channels. The total channel measures the total energy between 0.2 and 100  $\mu\text{m}$ . The shortwave channel (0.2–4  $\mu\text{m}$ ) is subtracted from the total channel to obtain the longwave part of the spectrum [21]. The fourth channel is an IR thermal channel (10.5–12.5  $\mu\text{m}$ ) which is used in this article (Fig. 2). The instrument operates nominally since the beginning of the mission and its operational performances are well in line with the specifications [22]–[24]. The nominal resolution of the ScaRaB footprint at nadir is 40 km and is detailed in [18].

The stability of the instrument is monitored by the CNES on a daily basis and so far, the Megha-Tropiques instruments have shown remarkable stability [25]. The use of geophysical targets like deep convective clouds (DCC) has been shown to be useful for geophysical calibration and cross-calibration of either broad radiometers [26], [27]. It is used here to showcase the relative stability of the channel 4 to that of the longwave channel. Fig. 3 shows the ratio between the radiance in channel 4 and channel 1 over the studied period for various deep convective regimes. The two channels of the instrument show no sign of relative degradation and a very steady behavior. Comparisons with the Clouds and the Earth's Radiant Energy System (CERES) instrument using dedicated collocation campaigns [28] further indicate a very good agreement between the two instruments' longwave channels [29].

246  
247  
248  
249  
250  
251  
252  
253  
254  
255  
256  
257  
258  
259  
260  
261  
262  
263  
264  
265  
266  
267  
268  
269  
270  
271  
272  
273  
274  
275  
276  
277  
278  
279  
280  
281  
282  
283  
284  
285

AQ:6

285

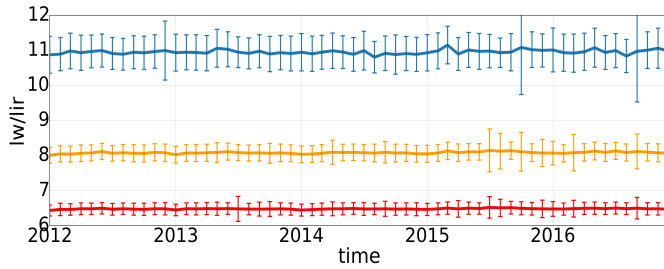


Fig. 3. Evolution of the ratio between measured radiance in the longwave band and in the IR channel of ScaRaB over the 2012–2016 period for various deep convective regimes. The blue curve corresponds to an IR radiance lower than  $2.25 \text{ W} \cdot \text{m}^{-2} \cdot \text{sr}^{-1}$  corresponding to a 187 K BT, the yellow one lower than  $4.25 \text{ W} \cdot \text{m}^{-2} \cdot \text{sr}^{-1}$  (207.4 K), and the red curve corresponds to an IR radiance lower than  $7.75 \text{ W} \cdot \text{m}^{-2} \cdot \text{sr}^{-1}$  (224.5 K).

286 The ScaRaB instrument is also thermally controlled and is not  
 287 impacted by icing events as shown in the monitoring of the  
 288 instrument performances [22], [23]. The combination of an  
 289 accurate and stable instrument makes it a well-suited reference  
 290 to adjust the geostationary data.

291 Here we use the so-called level 2B products that consist  
 292 of a  $0.5^\circ$  regularly gridded instantaneous directional radiances  
 293 ( $\text{W} \cdot \text{m}^{-2} \cdot \text{sr}^{-1}$ ). The original measurements are averaged on the  
 294 regular grid using a statistical technique and the point spread  
 295 function of the instrument [30]. Since 2011, the availability  
 296 of this product is about 99.9%, making it a useful resource as  
 297 a reference instrument for the spectral homogenization of the  
 298 GEORing data. Note that unlike sun-synchronous platforms,  
 299 the precessing orbit of Megha-Tropiques samples all the local  
 300 times every 51 days allowing the collocation with the geo-  
 301 stationary data all through the day and then the correction of  
 302 the midnight IR anomaly [10], [18], [31]. The low inclination  
 303 at the equator ( $20^\circ$ ) and high altitude of flight (865 km) also  
 304 allow high repetitive measurements in the tropics [18].

### 305 III. HOMOGENOUS LEVEL 1C IR DATA SET 306 FOR THE TROPICS FOR 2012–2016

#### 307 A. Homogenization of the Temporal Resolution

308 Given the requirements for cold cloud studies (see  
 309 Section I), the lack of temporal resolution homogeneity  
 310 between the geostationary imagers is accounted for by using  
 311 a 30-min temporal frequency for all the platforms, preventing  
 312 the use of MTSAT data in the southern hemisphere.

#### 313 B. Homogenization of the Spatial Resolution

314 A common equal angle grid of  $0.04^\circ \times 0.04^\circ$  has been  
 315 selected for all the platforms to account for this source of  
 316 inhomogeneity. This resolution is very close to the native  
 317 resolution of GOES-13, GOES-15, MTSAT-2, and Meteosat-7  
 318 data. The regridding process is performed by applying the  
 319 inverse distance weighting method in the radiance space with  
 320 a maximum search radius corresponding to the sum of half  
 321 of the geostationary spatial resolution for a given pixel plus  
 322 a half of the equal angle grid resolution. Then, the average  
 323 radiance is transformed in BT using the Planck function in  
 324 order to account for its nonlinearity.

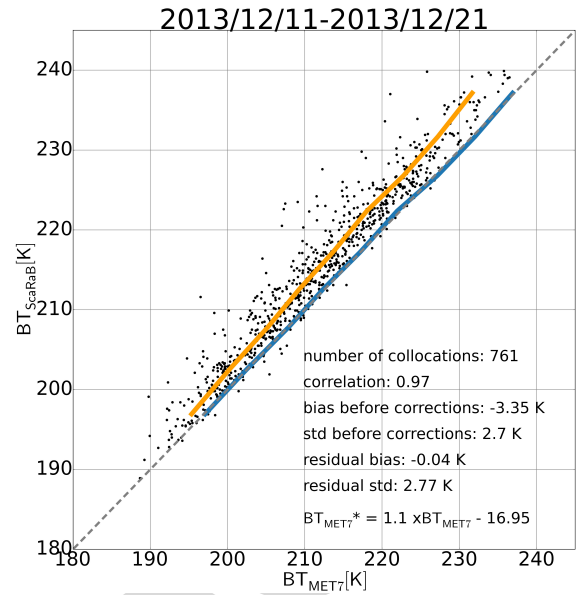


Fig. 4. Scatter plot between  $\text{BT}_{\text{MET7}}$  and  $\text{BT}_{\text{ScaRaB}}$  obtained after the filtering procedure over a ten-day period starting in 2013/12/11 for BT in the range [180–240 K]. The orange line corresponds to the average BT for each 5 K bin. The blue line corresponds to the residual bias.

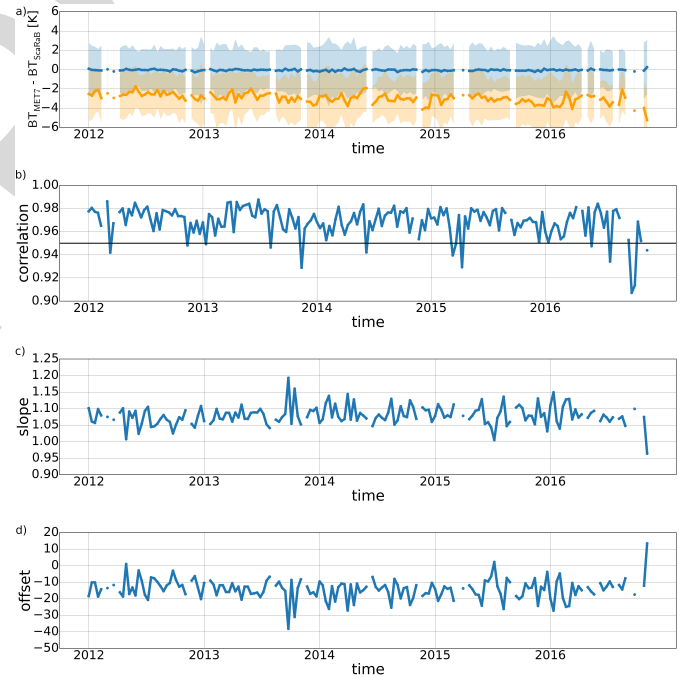


Fig. 5. (a) Time series of decadal initial BT bias (orange) and corrected BT bias (blue) for Meteosat-7 IR observations with respect to ScaRaB in the range [180–240 K]. The filled and transparent areas in orange and blue represent the standard deviations; (b) Time series of decadal linear regression correlations, (c) slope, and (d) offset between the ScaRaB and the Meteosat-7 IR observations in the range [180–240 K].

#### 325 C. Intercalibration and Spectral Normalization

326 1) *Regression Technique*: The use of a common low  
 327 earth-orbiting satellite, carrying an IR radiometer to anchor  
 328 each of the platforms to a common reference data set, forms  
 329 the basis of the different intercalibration and normalization  
 330



Fig. 6. (a) Time series of initial BT bias of geostationary IR observations with respect to ScaRaB in the range [180–240 K]. (b) Time series of BT bias between the geostationary IR observations and the ScaRaB observations in the range [180–240 K] after spectral and calibration corrections. (c) Time series of correlations between the ScaRaB and the geostationary IR observations in the range [180–240 K]. Each dot corresponds to a ten-day period.

efforts listed in Table I [14], [32] or under the GSICS calibration procedure [7]. Regression-based techniques are the most commonly used approaches. The difficulty arises in building the pairs (space/time/angular collocation) as well as in selecting the pairs of observations that will be regressed. This selection can have a strong impact on the result. Hence, it has been noted that the original ISCCP intercalibration was skewed toward a warm scene due to the implementation of the pairs selection filter prior to the regression computation, yielding a  $\sim 4$  K cold bias on the cold part of the spectrum [33]. Similarly, most of the tropical observations are located over large BT values and only a few of them are explained by DCCs. As the larger population of collocations is explained by high BT, the GSICS corrections are optimized for clear sky conditions and are not well suited for the cold cloud scenes [7]. A specific homogenization of the IR geostationary database is then required to fit with the objective of cold cloud tracking applications. This homogenization consists of a spectral normalization as well as an intercalibration of the various geostationary imagers focused on high cold clouds and on cold BTs. For this purpose, the BTs from the geostationary imagers are calibrated and spectrally normalized against the ScaRaB channel 4 measurements. The final data set then consists of a 10.5–12.5  $\mu\text{m}$  IR equivalent BT. Calibration uncertainty is expected to be within 1 K, which is the typical error for operational satellite calibration [34]. Contrary to other geostationary imagers, the correction of the Meteosat-7/MVIRI imager is restricted to an intercalibration procedure,

since its broad SRF is similar to the ScaRaB/channel 4 and both of them are centered on 11.5  $\mu\text{m}$ .

2) *Selection of the Data Match-Ups for the Regression:* The IR geostationary data from all the platforms are first remapped from their native formats to a regular lon/lat  $0.5^\circ$  grid every 30 min to allow direct comparison with the ScaRaB/L2B data. Prior to computing the averaged radiance and the associated spatial standard deviation for each  $0.5^\circ$  grid point, the BTs of each geostationary platform are converted in radiances ( $\text{mW} \cdot \text{m}^{-2} \cdot \text{sr}^{-1} \cdot \text{cm}^{-1}$ ) by applying the Planck function. The information on geostationary scan-time is also indicated for every grid point. The collocation between the ScaRaB-L2B observation and the IR  $0.5^\circ \times 0.5^\circ$  gridded geostationary data is reached when both view the same scene with a predefined time delay and similar viewing geometry. The predefined criteria are.

- 1) A maximum VZA of  $20^\circ$  and  $26^\circ$ , respectively, for the ScaRaB and the geostationary observation, to ensure alignment of the collocated pixels in viewing geometry and to avoid limb-darkening issues [35].
- 2) A maximum time delay of 10 min between two collocated pixels, which is a tradeoff between a relevant number of match-ups to populate the decadal regressions and the best possible temporal precision.
- 3) The IR-gridded radiances are regressed in units of temperature.

As we focus on high cold clouds scenes, we have developed a filtering procedure that keeps more collocation scenes at a colder temperature. Indeed, a bulk of collocations occurs at

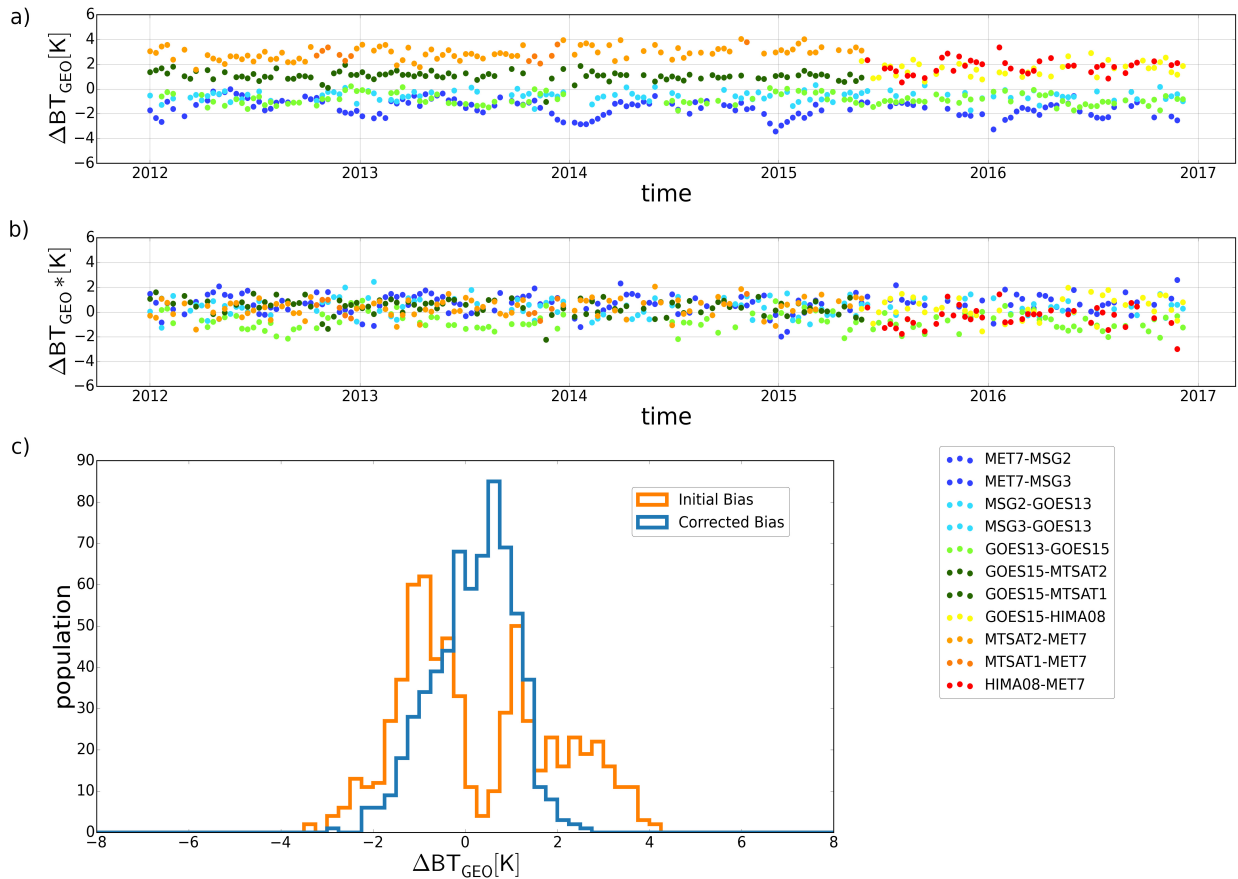


Fig. 7. (a) Time series of initial BT bias between pairs of geostationary platforms observing common areas with an equivalent VZA in the range [180–240 K]. (b) After spectral and calibration corrections; each dot corresponds to a ten-day period. (c) Distribution of the bias before and after corrections over the 2012–2016 period for all the pairs of geostationary platforms for all the ten-day periods.

386 a warmer temperature and displays a lower standard deviation [33]. To separate the high cold cloud population from  
 387 the warmer targets in the scatterplot, thresholds are applied to the GEO standard deviation that depends on the BT.  
 388 Pixels presenting a  $BT_{GEO} > 240$  K are rejected if their standard deviations are larger than 0.5 K and pixels with  
 389  $BT_{GEO} < 240$  K are kept if their standard deviations are lower than 2 K. Besides separating the high cold cloud popu-  
 390 lation from clear sky pixels, this filtering procedure ensures that heterogeneous moving objects do not contaminate the  
 391 collocation scenes and that the two instruments observe the same high cloud target. Assuming also that the IR radiometers  
 392 onboard geostationary platforms have a linear response when observing high cold cloud homogeneous scenes [8], [36],  
 393 the calibration and spectral normalization corrections are then based on linear regressions computed over a 180–240 K  
 394 range. For this, the collocated  $BT_{GEO}$  and  $BT_{ScaRaB}$  are binned and averaged for every  $BT_{ScaRaB}$  interval of 5 K from 180 to  
 395 240 K. The regression coefficients are then computed over these binned data every ten days and over a ten-day period.  
 396 This is required to ensure statistical robustness but prevent higher frequency variation (<10 days) of the calibration  
 397 issues (due to decontamination for instance) to be accounted for. As shown below, such higher frequency effects do not  
 398 impact the residuals of the regression. Correlations are used to  
 399  
 400  
 401  
 402  
 403  
 404  
 405  
 406  
 407  
 408  
 409  
 410

411 determine the ten-day period that might have match-ups errors. If the correlations are lower than 0.95 or if the population  
 412 of collocations does not exceed ten matchups, we consider that the linear regression cannot be computed and that every  
 413 ten-day period is removed from our analysis. In this case, the previous regression coefficients are replicated.  
 414  
 415  
 416

417 3) *Results*: Fig. 4 shows an example of such a regression computed from 761 collocated pixels between the Meteosat-7/  
 418 MVIRI imager and the Megha-Tropiques/ScaRaB observations acquired over a ten-day period from 2013/2012/2011 and  
 419 for a range between 180 and 240 K. The  $11.5 \mu\text{m}$  channel of Meteosat-7 exhibits a large negative bias ( $-3.35$  K) for  
 420 this considered BT and for this specific period. The blue line shows the regression fit given by a slope of 1.11 and  
 421 an offset of  $-16.95$  K. The correction has produced a very low residual bias, which averages at  $-0.04$  K over this  
 422 decadal period, and the correlation higher than 0.97 between the two data sets shows the high quality of the regression  
 423 computation. Fig. 5(a) shows the time series of difference between Meteosat-7/MVIRI and ScaRaB before and after  
 424 calibration over the 2012–2016 period. The Meteosat-7 BT is corrected every ten days using the slopes and offset com-  
 425 puted from the linear regression. Over the period and for the specific Meteosat-7 geostationary platform, 12% of the  
 426 decadal scatterplots are excluded from our analysis following  
 427  
 428  
 429  
 430  
 431  
 432  
 433  
 434  
 435

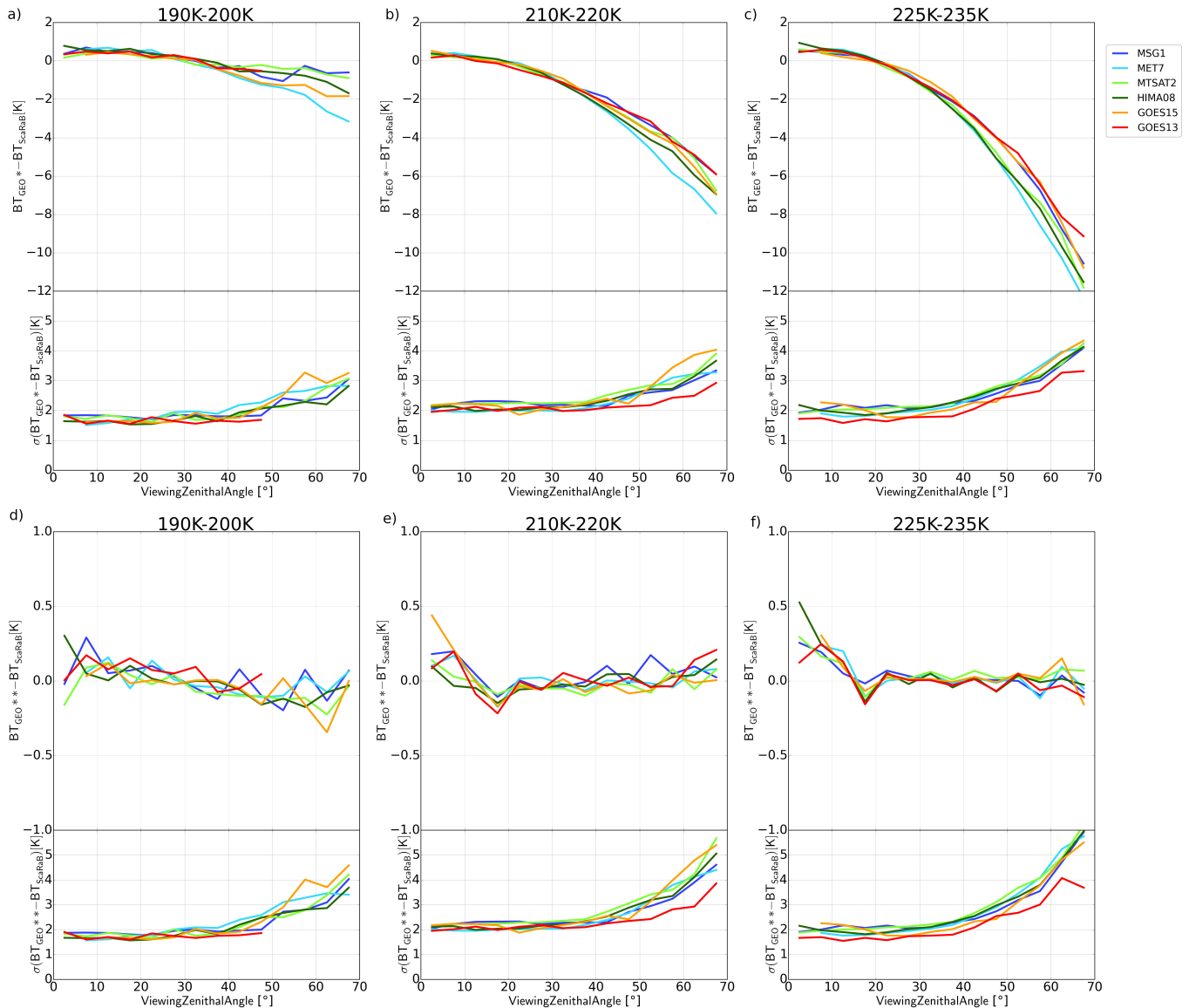


Fig. 8. Variation of the BT bias and the corresponding standard deviation between the GEO and the SCARAB observations according to the geostationary VZA, for a  $VZA_{ScaRaB} < 20^\circ$  and for three different ranges of  $BT_{ScaRaB}$ . (a)–(c) Before VZA corrections. (d)–(f) After VZA corrections.

the filtering procedure [Fig. 5(b)] and 87 405 collocations have then been used to compute the decadal regressions. One can observe that over the 2012–2016 period, and before the corrections, the Meteosat-7/MVIRI exhibits a negative bias, averaging at  $-2.98$  K and negatively increasing slightly with time due to contamination on the optics. This radiometric issue has been fully documented in [7]. The variations of the slopes and offsets are relatively stable over the period [Fig. 5(c) and (d)], showing the robustness of the methodology. After applying the calibration correction, the residual bias is very smooth, stable, and close to zero over the whole period. The calibration and spectral normalization corrections are applied on all the geostationary platforms available over the 2012–2016 period. The results have been obtained over the entire period, and for all the geostationary platforms by filtering 8% of the decadal scatterplots which did not pass our

quality control [Fig. 6(c)], leading to a comparison of around 655 000 collocations. Fig. 6(a) shows the time series of the decadal initial bias in BT for all the geostationary imagers with respect to the ScaRaB observations in the range 180–240 K. Over the 2012–2016 period, the Meteosat-7/MVIRI exhibits the highest error as discussed previously. It is also to be noted that the MSG/SEVIRI imager shows a relatively high negative bias ( $-1.39$  K) to be compared to the other instruments whose biases are mainly in the range  $-0.5$ – $0.5$  K over the entire period. While the calibration issues only explain the bias between Meteosat-7 and ScaRaB, the differences of temperature between ScaRaB and the other geostationary platforms can be explained by both a poor calibration and some differences in the SRF. The results of the intercalibration and spectral normalization are shown in Fig. 6(b). Over the entire period and for all the geostationary platforms, the decadal

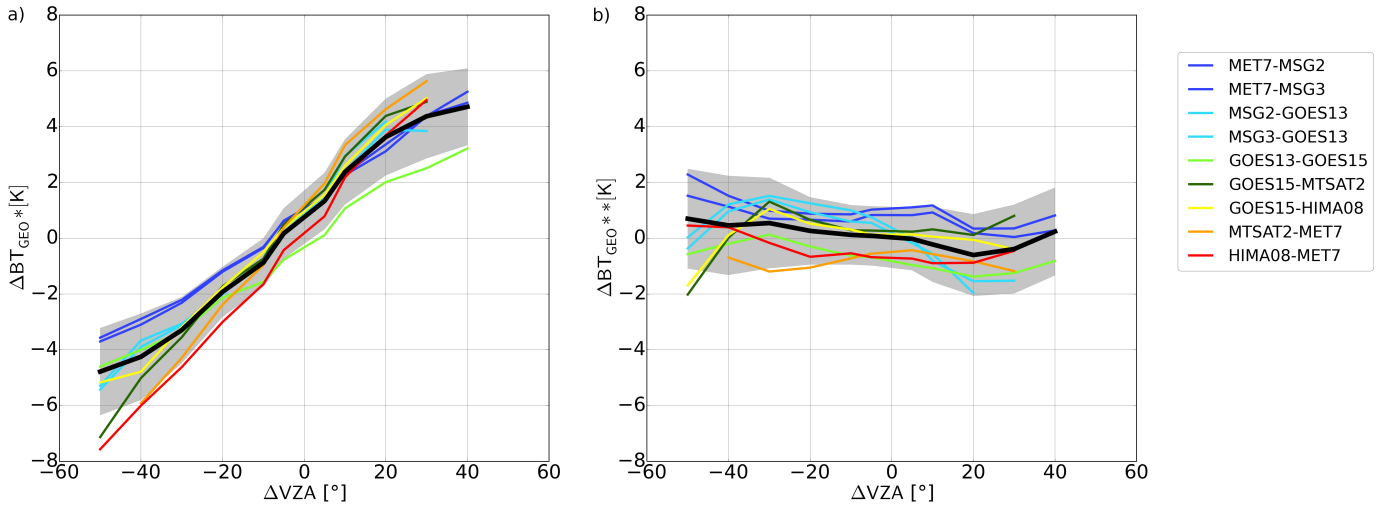


Fig. 9. Variation of the BT bias according to the VZA differences between pairs of geostationary platforms observing common areas and for  $BT_{ScaRaB}$  in the range [180–235 K]. (a) Before VZA corrections. (b) After VZA corrections. The BT bias and its standard deviation for all the pairs of geostationary platforms are represented respectively by the black line and the filled area in gray over the 2012–2016 period for all the ten days.

468 residual bias indicates a very low and stable bias, around 0 K,  
 469 with a standard deviation lower than 0.08 K between  $BT_{ScaRaB}$   
 470 and  $BT_{GEO}$ . The corrections are then directly applied to the  
 471 original geostationary data.

472 To fully describe the impact of the ScaRaB calibration  
 473 and spectral corrections, an independent validation has been  
 474 developed. The bias of uncorrected and corrected  $BT_{GEO}$  is  
 475 then computed in the range of 180–240 K every ten days  
 476 between pairs of neighbored geostationary platforms observing  
 477 common areas and sharing an equivalent VZA (Fig. 7). Indeed,  
 478 for two adjacent geostationary satellites, the BT bias at the  
 479 middle of the overlap region should average to zero, due to  
 480 the similar geometry for both platforms. Fig. 7(a) shows the  
 481 time series of decadal mean differences between uncorrected  
 482 BTs of each pair of geostationary satellites. Each color  
 483 represents a pair of geostationary platforms. Results indicate  
 484 a scatter of the decadal bias between  $-4$  and  $4$  K. The  
 485 maximum bias occurs for the BT differences between  
 486 MTSAT-1/2 and Meteosat-7, which averages at  $2.9$  K from  
 487 the beginning of 2012 to June 2015. The bias between  
 488 uncorrected  $BT_{MET-7}$  and  $BT_{MSG-1/2/3}$  exhibits a relatively  
 489 high bias ( $-1.62$  K on average) and is distinguishable from  
 490 the other pairs of geostationary satellites, in contrast to  
 491 its relatively high seasonal variations. The distribution of  
 492 the decadal initial bias for all the geostationary platforms  
 493 over the 2012–2016 period [Fig. 7(c)] reveals a multimodal  
 494 distribution, which averages at  $0.25$  K and displays a standard  
 495 deviation of  $1.65$  K. Fig. 7(b) shows that the corrections  
 496 applied to the geostationary IR observations improve the error  
 497 as well as the disparity of the scatter plot over the whole  
 498 period and for all the geostationary platforms. These results  
 499 are confirmed by the Gaussian distribution of the decadal  
 500 bias for corrected  $BT_{GEO}$  shown in Fig. 7(c), which averages  
 501 at  $0.19$  K with a standard deviation of  $0.87$  K. The resulting  
 502 geostationary satellite calibration residuals specifications are  
 503 hence well within the  $1$  K limit previously mentioned and

demonstrate the importance to develop a correction procedure  
 for the geostationary IR observations at cold temperatures.

#### D. Limb-Darkening Adjustment

1) *Methodological Considerations:* To complete the  
 homogenization procedure of the geostationary database, we  
 focus now on the dependence of the  $BT_{GEO}$  on the VZA.  
 This issue, also called limb darkening, corresponds to a  
 decrease in the temperature as the VZA increases. The greater  
 optical path length of the absorbing atmosphere, as the  
 VZA increases, results in a larger atmospheric absorption.  
 Indeed, a longer optical path length contains much more  
 water vapor and ozone explaining the observation of colder  
 temperatures [35], [37], [38]. Cloudy scenes imply a second  
 mechanism in the VZA issues [35]. A geometric effect may  
 also be involved when the sides of the clouds obstruct the  
 Earth’s emitted radiation at a large VZA. Some studies on  
 these geometric effects discussed the different configurations  
 of cloud fields [39]. To prevent an erroneous analysis between  
 meteorological situations, which occurred at nadir and at a  
 large VZA, the BTs have to be limb-adjusted. Some studies  
 have been carried out to limb adjust the IR observations  
 for cloudy regions by establishing empirical limb correction  
 functions, depending on the cosine of zenith angle from the  
 radiative transfer model for low earth orbit platforms [39]  
 and IR geostationary observations [40]. However, it has  
 been shown [41] that the corrections developed by [39]  
 underestimate the observed BTs. The variation of the radiance,  
 according to the zenith angle, is approximated in the CLAUS  
 data set, by applying a function of the cosine of the zenith  
 angle. Another way to face the limb-darkening issues is to use  
 observations from low earth orbit platforms. Limb-correction  
 algorithms have been developed for microwave observations  
 from the AMSU-A and are based on a physical-statistical  
 methodology [37]. The limb-darkening problem has also been

504  
 505

506

507  
 508  
 509  
 510  
 511  
 512  
 513  
 514  
 515  
 516  
 517  
 518  
 519 AQ:7

520

521  
 522  
 523  
 524  
 525  
 526  
 527  
 528  
 529  
 530  
 531  
 532  
 533  
 534  
 535  
 536  
 537

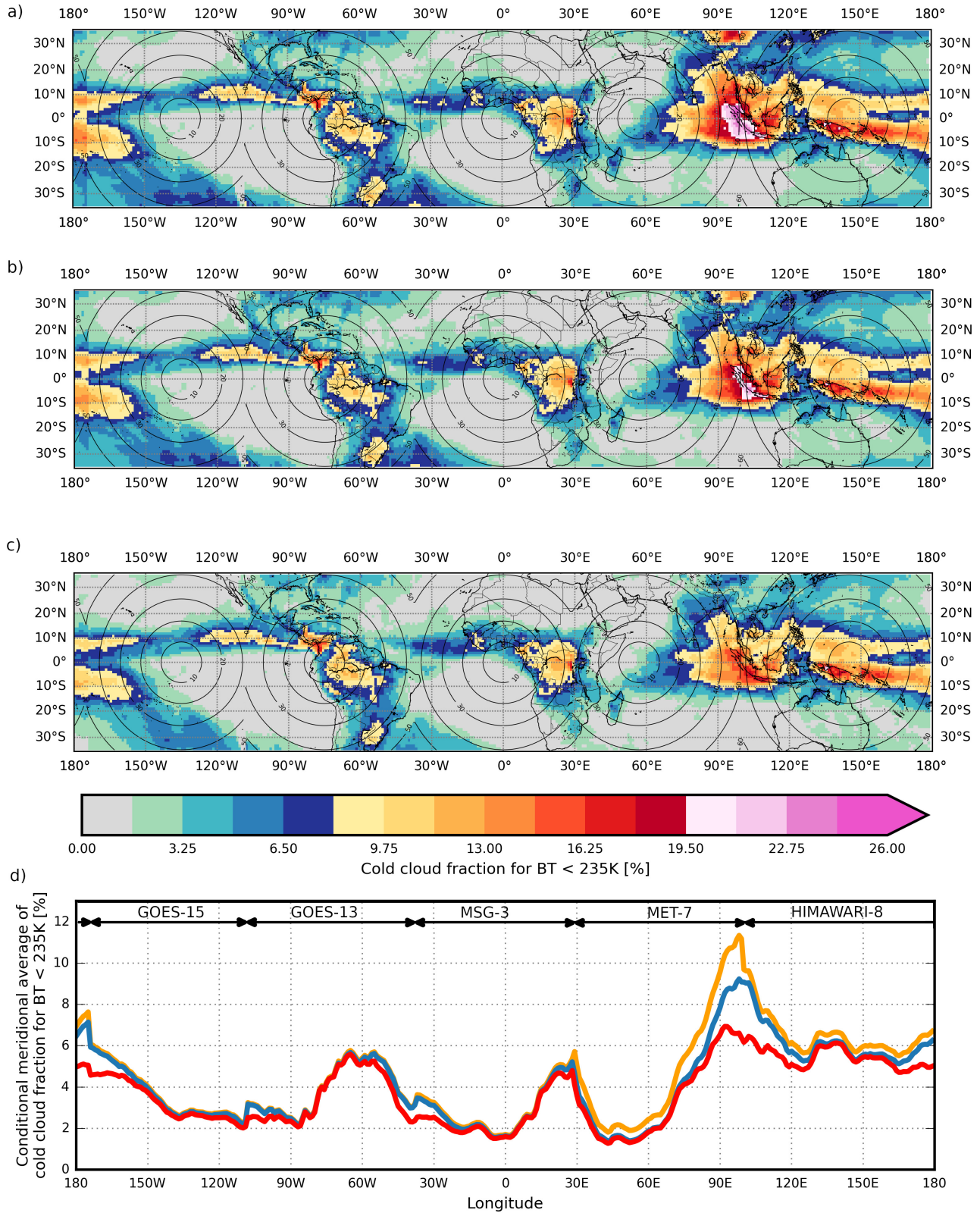


Fig. 10. Map of the mean cold cloud fraction (%) for  $BT_{GEO} < 235K$  over 2016 (a) by using the initial  $BT_{GEO}$  before any corrections, (b) by using the calibrated and spectrally corrected  $BT_{GEO}$ , and (c) after applying the VZA corrections on  $BT_{GEO}$ . The black circles represent the different levels of VZA. (d) Conditional meridional average of the cold cloud fraction for  $BT_{GEO} < 235K$  before any corrections (orange line), after applying the calibration and spectral corrections (blue line) and after applying the VZA corrections (red line).

538 explored by comparing the radiances from the geostationary  
 539 platforms with observations from polar orbiter platforms [40].  
 540 Some limb-darkening corrections have been computed from

collocated pairs of GOES platforms (GOES-8/GOES-10) 541  
 and Meteosat platforms (Meteosat-5/Meteosat-7) [35]. They 542  
 proposed a two-step correction. First, a correction table of 543

544 the  $BT_{GEO}$  as a function of VZA is applied to  $BT_{GEO}$  only  
 545 for observations in the tropics. For mid-latitude regions,  
 546 an additional correction is applied to tackle the latitudinal  
 547 and seasonal dependence of  $BT_{GEO}$ . This dependence is  
 548 explained by a smaller contrast between the cloud top and  
 549 the Earth's surface in mid-latitudes than over the tropics.  
 550 This limb-darkening correction is used in GridSat and ISCCP  
 551 data sets [4]. However, this methodology is likely to suffer  
 552 from limitations to be used to homogeneously limb adjust a  
 553 fleet of geostationary satellites. Indeed, the limb adjustment,  
 554 developed in the 2000s and empirically derived from a  
 555 combination of a specific and limited set of instruments,  
 556 may also be biased for other and new generation of  
 557 geostationary instruments [12]. Moreover, the computation of  
 558 the limb-darkening correction is limited by the range of VZA,  
 559 due to the combination of the fixed location of geostationary  
 560 satellites inducing few observations of cold  $BT_{GEO}$ .

561 It appears important, for this article, to tackle limb-  
 562 darkening issues on geostationary satellite per geostationary  
 563 satellite over the full time period by using a common reference,  
 564 such as the IR observation from the ScaRaB instrument.  
 565 This correction focuses on cold clouds monitored by the IR  
 566 imagery of geostationary satellites previously intercalibrated  
 567 and normalized into a  $10.5\text{--}12.5\ \mu\text{m}$  IR equivalent BT, called  
 568  $BT_{GEO}^*$ . For this purpose, we perform for each GEO platform  
 569 a collocation procedure between the regular lon/lat  $0.5^\circ$  and  
 570 corrected IR geostationary data, presented previously, and the  
 571 ScaRaB/L2B IR observation over the entire 2012–2016 period.  
 572 The collocation procedure is applied under some criteria.  
 573 Where the zenithal angles of ScaRaB do not exceed  $20^\circ$ ,  
 574 the geostationary zenith angles can range from  $0^\circ$  to  $70^\circ$ . The  
 575 collocation is also performed with a time delay of less than  
 576 10 min between the GEO and the ScaRaB observations and for  
 577  $BT_{ScaRaB}$ , which does not exceed 235 K for standard deviations  
 578 lower than 2 K.

579 GEO-ScaRaB match-ups are binned into geostationary  
 580 zenith angle intervals of  $2^\circ$  and for zenith angles ranging  
 581 from  $20^\circ$  to  $70^\circ$ . For GEO VZAs lower than  $20^\circ$ , a unique  
 582 limb correction is performed. Moreover, to ensure a relevant  
 583 sample size on each  $2^\circ$  zenith angle bin, the regressions are  
 584 applied annually. For each zenith angle interval, the collocated  
 585  $BT_{GEO}^*$  and  $BT_{ScaRaB}$  are binned and averaged for every  
 586  $BT_{ScaRaB}$  interval of 5 K, from 180 to 235 K. To filter corrupted  
 587 collocated points, the binning procedure is performed when  
 588 at least ten samples are present. The limb correction then  
 589 consists of applying annual regressions between the binned  
 590 GEO and ScaRaB data for every  $2^\circ$  zenith angle bin and  
 591 for each geostationary platform. A second-order polynomial  
 592 regression has been preferred over the linear regression, due  
 593 to slight improvements in the minimization of the residuals.

594 2) *Results*: Fig. 8(a)–(c) shows the variation of the initial  
 595 bias between each GEO platform and ScaRaB, according  
 596 to the VZA for different bins of ScaRaB temperatures and  
 597 over the 2012–2016 period. First, one can observe a negative  
 598 increase in the bias as the VZA increases, whatever the range  
 599 of BT. For VZA lower than  $30^\circ$ , the absolute bias seems to be  
 600 lower than 1 K, whatever the  $BT_{ScaRaB}$  is. However, we can  
 601 observe drastic differences in the bias evolution depending on

the  $BT_{ScaRaB}$  bin. Indeed, at warmer  $BT_{ScaRaB}$  [225–235 K],  
 the negative increase in the bias according to the VZA is more  
 pronounced than for colder values of  $BT_{ScaRaB}$  [190–200 K].  
 For a VZA at  $40^\circ$ , the bias averages at  $-0.63$  K for  $BT_{ScaRaB}$ ,  
 ranging from 190 to 200 K and for all the GEO platforms,  
 while the bias averages at  $-2.9$  K for  $BT_{ScaRaB}$  greater than  
 225 K and for a similar VZA. It is also to be noticed that  
 the disparity of the bias among GEO platforms increases with  
 the VZA. Thus, at a  $60^\circ$  zenith angle and for the 225–235 K  
 range, the bias varies from  $-7.4$  to  $-9.5$  K for GOES-15 and  
 Meteosat-7, respectively. Such large errors have been previ-  
 ously reported for an older Meteosat first-generation satellite  
 (Meteosat-4) compared to NOAA/AVHRR reference [27].  
 Note that the uncertainty does not increase much with the BT  
 but increases with the VZA. Fig. 8(d)–(f) shows the results  
 of the limb-darkening corrections according to the variation  
 of the zenith angle for all the geostationary platforms and for  
 different ranges of  $BT_{ScaRaB}$ . Over the whole range of ScaRaB  
 BTs, the residual biases average at 0 K, regardless of the  
 geostationary platform and the zenith angles. These results  
 demonstrate the capability of the limb-darkening correction  
 methodology we have developed. An independent validation  
 is provided in Fig. 9 by comparing pairs of geostationary  
 platform observations. It shows the variation of the decadal  
 biases of  $BT_{GEO}^*$  between pairs of geostationary satellites,  
 according to the difference of their VZAs ( $\Delta VZA$ ), before  
 and after applying limb-darkening corrections. A  $\Delta VZA$  of  
 $0^\circ$  means that two adjacent geostationary platforms observe  
 the same region with an equivalent VZA. On the contrary,  
 a large  $\Delta VZA$  indicates that a given geostationary platform  
 observes a region with a nadir zenith angle, while the adjacent  
 geostationary platform monitors the same region with a limb  
 zenith angle. Before applying the zenith angle corrections,  
 we can observe an increase of  $BT_{GEO}^*$  bias for all the  
 platforms from  $\sim -5$  to  $\sim 5$  K as the  $\Delta VZA$  moves from  
 $-50^\circ$  to  $40^\circ$  [Fig. 9(a)]. The standard deviation, on its side,  
 varies between 0.86 K for a low  $\Delta VZA$  and 1.57 K for  
 large  $\Delta VZA$ . Results indeed indicate a larger disparity of  
 the  $BT_{GEO}^*$  biases between pairs of geostationary satellites  
 for large  $\Delta VZA$ . After applying the zenith angle correction  
 [Fig. 9(b)], the  $BT_{GEO}^{**}$  bias is relatively stable and averages  
 at 0.09 K with a standard variation of 1.43 K, regardless of  
 the variation of  $\Delta VZA$ . The standard deviation varies from  
 1.05 to 1.78 K for low and large  $\Delta VZA$ , respectively. Note  
 that when the limb-darkening issue is clearly improved and  
 corrected, the standard deviation for a low VZA is a little  
 larger than before applying the VZA correction.

#### IV. DISCUSSION AND CONCLUSION

In summary, a level 1c IR GEOing data set is introduced.  
 This data set is a consistent  $10.5\text{--}12.5\ \mu\text{m}$  IR equivalent BT  
 data set, with a homogeneous recalibration, a  $0.04^\circ \times 0.04^\circ$   
 spatial resolution, a 30 min common time resolution, and a  
 correction for limb effect. The data set covers the 2012–2016  
 period. The global homogeneity of the IR GEOing data set,  
 regardless of the variation of VZA, is then characterized by a  
 standard deviation of 1.43 K within any of two geostationary  
 satellites.

As discussed in the Introduction section, global geostationary IR observations provide useful resources to carry out studies on convective systems. Cold cloud tracking algorithms usually delineate cold clusters by applying a 235 K threshold on IR geostationary data. To evaluate the impact of the geostationary IR data homogenization on high cold clouds, we compute the cold cloud fraction. The fraction is determined by applying a 235 K threshold on the initial  $BT_{GEO}$  before any corrections, on the spectrally adjusted and calibrated  $BT_{GEO}$  and finally on the VZA corrected IR data for the 2016 period and over the entire tropics. The computations are performed by using the selected configuration of the geostationary fleet and the map of cold cloud fraction provided on a  $1^\circ \times 1^\circ$  grid [Fig. 10(a)–(c)]. Before corrections, a local maximum of cold cloud fraction reaching 26% is seen in the Meteosat-7 area over the west coast of the Indo–China peninsula. However, the calibration correction allows to attenuate this fraction which falls to 22%. Also, note that this region is observed by Meteosat-7 with a VZA of  $47^\circ$ . After the limb-adjustment procedure, the value of cold cloud fraction for this specific region decreases to 17%. The maximum of cold cloud fraction is now located over the warm pool and is observed by the HIMAWARI-8 platform. One can also see that the local maximum of cold cloud fraction over the Tibetan plateau is strongly attenuated with all the corrections. Before applying the homogenization procedure, one can observe some steps of the conditional meridional average of cold cloud cover at the boundary of Meteosat-7 and HIMAWARI-8 and between HIMAWARI-8 and GOES-15, reaching 1.65% and 1.47%, respectively [Fig. 10(d)]. The combined corrections improve these issues and show a cold cloud cover exhibiting a smoother transition from one platform to another. Fig. 10(d) shows similar cold cloud covers for low VZA between a unique calibration/spectral correction and the combined calibration/spectral and VZA corrections, while one can observe a decrease in cold cloud cover for large VZA between the two corrections.

The extension of the current database beyond 2016 is under consideration. The configuration of the fleet, nevertheless, drastically changes in 2017 with the end of operation of Meteosat-7 and the arrival of MSG-1 in February on a shifted position, although not fully covering the Indian Ocean. Tests are needed to explore the sensitivity of the database to this new configuration. The use of INSAT-3D is also contemplated as a better way to bridge MSG-1 and HIMAWARI-8 data. GOES-R has become operational and the stream of GOES-16 replaces GOES-13 in December 2017. Similarly, GOES-17 is now operational as the new GOES west coverage replacing the GOES-15 platform from February 2019.

Up to the end of 2018, the Megha-Tropiques mission has been operated nominally granting the possibility of extending the present effort up to that time. While the present work relies on the ScaRaB instrument onboard Megha-Tropiques, it can easily be applied to alternative IR reference observations, from hyperspectral sounders, for instance. This article indicates that the final calibrated and limb-adjusted IR observations for  $BT < 240$  K can be homogeneous throughout the GEOring

with less than 1.5 K standard deviation, and that further future efforts should strive for such, or better, accuracy.

#### ACKNOWLEDGMENT

The authors would like to thank the ESPRI/IPSL team for providing computing and storage resources. They also thank the DWD as well as the French data center AERIS for their help in accessing the data (GEOring, ScaRaB). They also thank G. Urbani and C. Bovalo for their help in handling the geostationary satellite data archive. They further acknowledge M. Dejus, Project Manager at CNES, and his team for their help on the technical aspects of ScaRaB. The ScaRaB L2B is available in the ICARE data and service center with an *Anonymous File Transfer Protocol* ([ftp://ftp.icare.univ-lille1.fr/SPACEBORNE/SCARAB/MT1\\_L2B-FLUX-SCASL1A2\\_0.5deg.v2.01/](ftp://ftp.icare.univ-lille1.fr/SPACEBORNE/SCARAB/MT1_L2B-FLUX-SCASL1A2_0.5deg.v2.01/)). The calibration coefficients and the limb-adjustment coefficients are available at the following DOI: <https://doi.org/10.14768/20191125>.

#### REFERENCES

- R. A. Schiffer and W. B. Rossow, "The International Satellite Cloud Climatology Project (ISCCP): The first project of the World Climate Research Programme," *Bull. Amer. Meteorol. Soc.*, vol. 64, no. 7, pp. 779–784, Jul. 1983.
- M. L. Salby, H. H. Hendon, K. Woodberry, and K. Tanaka, "Analysis of global cloud imagery from multiple satellites," *Bull. Amer. Meteorol. Soc.*, vol. 72, no. 4, pp. 467–480, Apr. 1991.
- G. J. Huffman *et al.*, "The Global Precipitation Climatology Project (GPCP) combined precipitation dataset," *Bull. Amer. Meteorol. Soc.*, vol. 78, no. 1, pp. 5–20, 1997.
- K. R. Knapp *et al.*, "Globally Gridded Satellite observations for climate studies," *Bull. Amer. Meteorol. Soc.*, vol. 92, no. 7, pp. 893–907, Jul. 2011.
- R. A. Kohrs, M. A. Lazzara, J. O. Robaidek, D. A. Santek, and S. L. Knuth, "Global satellite composites—20 years of evolution," *Atmos. Res.*, vols. 135–136, pp. 8–34, Jan. 2014.
- P. Zhang, K. Holmlund, M. Goldberg, and J. Lafeuille, "The Global Space-based Inter-Calibration System (GSICS)," in *Proc. IEEE Int. Geosci. Remote Sens. Symp. (IGARSS)*, Jul. 2016, pp. 5522–5523.
- T. J. Hewison *et al.*, "GSICS inter-calibration of infrared channels of geostationary imagers using Metop/IASI," *IEEE Trans. Geosci. Remote Sens.*, vol. 51, no. 3, pp. 1160–1170, Mar. 2013.
- D. R. Doelling *et al.*, "Geostationary enhanced temporal interpolation for CERES flux products," *J. Atmos. Ocean. Technol.*, vol. 30, no. 6, pp. 1072–1090, Jun. 2013.
- T. J. Hewison and J. Muller, "Ice contamination of Meteosat/SEVIRI implied by intercalibration against Metop/IASI," *IEEE Trans. Geosci. Remote Sens.*, vol. 51, no. 3, pp. 1182–1186, Mar. 2013.
- B. Scarino, D. R. Doelling, C. Haney, K. Bedka, and P. Minnis, "Utilizing the precessing orbit of TRMM to produce hourly corrections of geostationary infrared imager data with the VIRS sensor," *Proc. SPIE*, vol. 10403, Aug. 2019, Art. no. 104030H.
- G. J. Robinson and K. I. Hodges, "Cloud archive user service user guide," Tech. Rep., 2005, p. 16.
- K. R. Knapp, "Gridded satellite B1 FCDR—Monthly means," Tech. Rep., 2016.
- J. E. Janowiak, R. J. Joyce, and Y. Yarosh, "A real-time global half-hourly pixel-resolution infrared dataset and its applications," *Bull. Amer. Meteorol. Soc.*, vol. 82, no. 2, pp. 205–217, Feb. 2001.
- Y. Desormeaux, W. B. Rossow, C. L. Brest, and G. G. Campbell, "Normalization and calibration of geostationary satellite radiances for the International Satellite Cloud Climatology Project," *J. Atmos. Ocean. Technol.*, vol. 10, no. 3, pp. 304–325, Jun. 1993.
- T. Fiolleau and R. Roca, "An algorithm for the detection and tracking of tropical mesoscale convective systems using infrared images from geostationary satellite," *IEEE Trans. Geosci. Remote Sens.*, vol. 51, no. 7, pp. 4302–4315, Jul. 2013.

716  
717  
718  
719  
720  
721  
722  
723  
724  
725  
726  
727  
728  
729  
730  
731  
732  
733  
734  
735  
736  
737  
738  
739  
740  
741  
742  
743  
744  
745  
746  
747  
748  
749  
750  
751  
752  
753  
754  
755  
756  
757  
758  
759  
760  
761  
762  
763  
764  
765  
766  
767  
768  
769  
770  
771  
772  
773  
774  
775  
776  
777  
778  
779  
780

[16] M. Schröder, M. König, and J. Schmetz, “Deep convection observed by the Spinning Enhanced Visible and Infrared Imager on board Meteosat 8: Spatial distribution and temporal evolution over Africa in summer and winter 2006,” *J. Geophys. Res.*, vol. 114, no. D5, pp. 1–14, 2009.

[17] B. E. Mapes and R. A. Houze, “Cloud clusters and superclusters over the oceanic warm pool,” *Monthly Weather Rev.*, vol. 121, no. 5, pp. 1398–1416, May 1993.

[18] R. Roca *et al.*, “The Megha-Tropiques mission: A review after three years in orbit,” *Frontiers Earth Sci.*, vol. 3, p. 17, May 2015.

[19] R. Kandel *et al.*, “The ScaRaB earth radiation budget dataset,” Natural Resour. Canada/ESS/Sci. Tech. Publishing Services, Tech. Rep., 1998.

[20] J.-P. Duvel *et al.*, “The ScaRaB-Resurs Earth radiation budget dataset and first results,” *Bull. Amer. Meteorol. Soc.*, vol. 82, no. 7, pp. 1397–1408, Jul. 2001.

[21] M. Viollier and P. Raberanto, “Radiometric and spectral characteristics of the ScaRaB-3 instrument on Megha-Tropiques: Comparisons with ERBE, CERES, and GERB,” *J. Atmos. Ocean. Technol.*, vol. 27, no. 3, pp. 428–442, Mar. 2010.

[22] A. Rosak, T. Tremas, N. Karouche, L. Gillot, and O. Simonella, “Radiometric and geometric Scarab-Megha-Tropiques ground calibration comparison with first in orbit calibration,” in *Proc. IEEE Int. Geosci. Remote Sens. Symp.*, Jul. 2012, pp. 4746–4749.

[23] N. Karouche, C. Goldstein, A. Rosak, C. Malassingne, and G. Raju, “MEGHA-TROPIQUES satellite mission: In flight performances results,” in *Proc. IEEE Int. Geosci. Remote Sens. Symp.*, Jul. 2012, pp. 4684–4687.

[24] T. L. Trémas, N. Karouche, A. Rosak, A. Meygret, O. Aznay, and E. Hillairet, “ScaRaB: First results of the scanner for radiative budget on board the Indo-French satellite Megha-Tropiques,” *Proc. SPIE*, vol. 8510, Oct. 2012, Art. no. 851002.

[25] R. Roca *et al.*, “Le bilan scientifique de la mission Megha-Tropiques après 8 ans dans l’espace,” *La Météorologie*, no. 107, p. 36, 2019.

[26] J. P. Duvel and P. Raberanto, “A geophysical cross-calibration approach for broadband channels: Application to the ScaRaB experiment,” *J. Atmos. Ocean. Technol.*, vol. 17, no. 12, pp. 1609–1617, Dec. 2000.

[27] D. R. Doelling, D. Morstad, B. R. Scarino, R. Bhatt, and A. Gopalan, “The characterization of deep convective clouds as an invariant calibration target and as a visible calibration technique,” *IEEE Trans. Geosci. Remote Sens.*, vol. 51, no. 3, pp. 1147–1159, Mar. 2013.

[28] G. L. Smith, Z. P. Szewczyk, K. J. Priestley, and R. Roca, “Method of comparing CERES and ScaRaB 3 measurements,” in *Proc. Sensors, Syst., Next-Gener. Satellites XVI SPIE*, 2012, pp. 7193–7196.

[29] T. L. Trémas, O. Aznay, and O. Chomette, “ScaRaB and CERES-Terra: Results of the inter-comparison campaigns,” *Proc. SPIE*, vol. 9973, Sep. 2016, Art. no. 99730B.

[30] N. Gif, O. Chomette, and P. Raberanto, “Co-location algorithms geophysical data projection using pixel point spread function,” Megha-Tropiques Tech. Memo. 2, 2011.

[31] M. Capderou, “Sampling. Comparison with other Meteorological Satellites,” Megha-Tropiques Tech. Memo. 1, 2009.

[32] C. L. Brest, W. B. Rossow, and M. D. Roiter, “Update of radiance calibrations for ISCCP,” *J. Atmos. Ocean. Technol.*, vol. 14, no. 5, pp. 1091–1109, Oct. 1997.

[33] K. R. Knapp, “Calibration assessment of ISCCP geostationary infrared observations using HIRS,” *J. Atmos. Ocean. Technol.*, vol. 25, no. 2, pp. 183–195, Feb. 2008.

[34] M. König, J. Schmetz, and S. Tjemkes, “Satellite intercalibration of IR window radiance observations,” *Adv. Space Res.*, vol. 23, no. 8, pp. 1341–1348, Jan. 1999.

[35] R. Joyce, J. Janowiak, and G. Huffman, “Latitudinally and seasonally dependent zenith-angle corrections for geostationary satellite IR brightness temperatures,” *J. Appl. Meteorol.*, vol. 40, no. 4, pp. 689–703, Apr. 2001.

[36] T. H. von der Haar and S. Q. Kidder, *Satellite Meteorology—An Introduction*. New York, NY, USA: Academic, 1995.

[37] M. D. Goldberg, D. S. Crosby, and L. Zhou, “The limb adjustment of AMSU—A observations: Methodology and validation,” *J. Appl. Meteorol.*, vol. 40, no. 1, pp. 70–83, Jan. 2001.

[38] Q. Liu and F. Weng, “Uses of NOAA-16 and -18 satellite measurements for verifying the limb-correction algorithm,” *J. Appl. Meteorol. Climatol.*, vol. 46, no. 4, pp. 544–548, Apr. 2007.

[39] P. Minnis, “Viewing zenith angle dependence of cloudiness determined from coincident GOES east and GOES west data,” *J. Geophys. Res.*, vol. 94, no. D2, pp. 2303–2320, 1989.

[40] N. J. Elmer, E. Berndt, and G. J. Jedlovec, “Limb correction of MODIS and VIIRS infrared channels for the improved interpretation of RGB composites,” *J. Atmos. Ocean. Technol.*, vol. 33, no. 5, pp. 1073–1087, May 2016.

[41] K. I. Hodges, D. W. Chappell, G. J. Robinson, and G. Yang, “An improved algorithm for generating global window brightness temperatures from multiple satellite infrared imagery,” *J. Atmos. Ocean. Technol.*, vol. 17, no. 10, pp. 1296–1312, Oct. 2000.



**Thomas Fiolleau** received the Ph.D. degree from Ecole Polytechnique, Paris, France, in 2010 with a thesis on the use of satellite observation to study mesoscale convective systems in the framework of the Megha-Tropiques Indo-French Satellite Mission.

He was an Associate Engineer with the Laboratoire de Météorologie Dynamique (LMD), Paris, for two years. He worked as a United Nations Educational, Scientific and Cultural Organization (UNESCO) Consultant with the Centro Nacional de Monitoramento e Alertas de Desastres Naturais (CEMADEN), Brazil, a Brazilian operational center, where he worked on the development of operational algorithms to forecast convective systems. After two years at CNRM (joint laboratory between CNRS and Météo-France), he joined the CNRS in 2016 as a Research Engineer with the Laboratoire d’Etudes en Géographie et Océanographie Spatiales, Toulouse, France. His areas of specialization are remote sensing, image processing, tropical climate and meteorology, and his researches interests are focused on the development of cloud tracking algorithms from geostationary satellites and the study of the life cycle of tropical mesoscale convective systems by using satellite observations.



**Rémy Roca** received the M.S. degree in fundamental physics, with major in remote sensing, and the Ph.D. degree in 2000 from Université Paris, Paris, France, with a thesis on the use of satellite observations to evaluate climate models.

He was with the Scripps Institution of Oceanography, University of California, San Diego, CA, USA, for almost two years where he got familiar with image processing and cloud detection and tracking algorithms from geostationary satellites. From 2001 to 2012, he was with the Laboratoire de Météorologie Dynamique, Institut Pierre et Simon Laplace, Paris, where he was a CNRS Researcher. He was appointed a Mission Scientist of the Megha-Tropiques Indo-French Satellite Mission and took over the Piship of the mission in 2007. He is a Senior CNRS Researcher with the Laboratoire d’Etudes en Géographie et Océanographie Spatiales, Toulouse, France. His broad interests are focused on the study of the water cycle in the tropics and the use of satellite observations to investigate the tropical variability. He has more than 15 years of experience in the field of tropical climate, meteorology, and remote sensing.

Dr. Roca was the Chairman of the International Precipitation Group in 2014 and 2015, and since 2016, he has been co-leading the GEWEX/WCRP Data Analysis Panel.



**Sophie Cloché** received the M.S. degree in fundamental physics, with a specialization in remote sensing, and the Ph.D. degree in 1996 with a thesis on the use of satellite observations (POLDER) for cloud and water vapor detection from Université Paris, Paris, France.

From 1996 to 1998, she was a Post-Doctoral Position with the Laboratoire de Météorologie Dynamique (LMD/CNRS), Paris, working on narrow to broadband conversion to estimate the radiative fluxes. From 1998 to 2001, she was as a Research Engineer, on database management for the INDOEX program, LMD. In 2001, she obtained a fix position with the CNRS, Institut Pierre-Simon Laplace (IPSL), Paris, as Research Engineer, and also involved in database management for different national and international projects (AMMA, Hymex, GEWEX-Cloud Assessment for example). She is the Co-ordinator of the scientific ground segment for the Megha-Tropiques mission and involved in the CM SAF from Eumetsat for the development of a global precipitation product. She also coordinates space activities at IPSL and she is responsible of the database management of observations at IPSL.

AQ:9

AQ:10

AQ:11

856  
857  
858  
859  
860  
861  
862  
863  
864  
865  
866  
867  
868  
869  
870  
871  
872  
873  
874  
875  
876  
877  
878  
879  
880  
881  
882  
883  
884  
885  
886  
887  
888  
889  
890  
891  
892  
893  
894  
895  
896  
897  
898  
899  
900  
901  
902  
903  
904  
905  
906  
907  
908  
909  
910  
911  
912  
913  
914  
915  
916  
917  
918  
919  
920  
921  
922  
923  
924  
925  
926  
927

AQ:12

AQ:13

928  
929  
930  
931  
932  
933  
AQ:14 934  
935  
936  
937  
938  
939  
940  
941  
942  
943  
944



**Dominique Bouniol** received the Ph.D. degree from the University of Paris, Paris, France, in 2000, with a thesis on process-oriented use of observational data sets for understanding mesoscale storm deepening.

After 18 months in the Radar Meteorology Group, University of Reading, Reading, England, she joined the CNRS as a Researcher in 2002, first in CETP where she was involved in the implementation and exploitation of ground-based cloud radar in the framework of the Cloudnet project. She led the deployment of the airborne version of the cloud radar

within the AMMA experiment in Niger and Senegal, in 2006. While she was with CNRS, she joined the CNRM (joint laboratory between CNRS and Météo-France), in 2006, where her research focuses on physical processes involved in the tropical mesoscale convective system life cycle and more generally on tropical cloud processes using both observations and modeling tools.



**Patrick Raberanto** received the Ph.D. degree in astronomy and space technology from Paul Sabatier University, Toulouse, France, in 1984.

In 1990, he joined the Laboratoire de Météorologie Dynamique (LMD), Ecole Polytechnique, Paris, as a CNRS Research Engineer and was implied in the ScaRaB project. In the framework of the Megha-Tropiques mission, he was in charge of the ScaRaB calibration, validation, and the development of the ScaRaB level-2 products. His research interests include radiometric calibration and radiative budget observation.

945  
946  
947  
948  
949  
950  
951  
952  
953  
954  
955  
956

IEEE Proof

## AUTHOR QUERIES

### AUTHOR PLEASE ANSWER ALL QUERIES

**PLEASE NOTE:** We cannot accept new source files as corrections for your article. If possible, please annotate the PDF proof we have sent you with your corrections and upload it via the Author Gateway. Alternatively, you may send us your corrections in list format. You may also upload revised graphics via the Author Gateway.

- 1) Please be aware that authors are required to pay overlength page charges (\$230 per page) if the article is longer than 6 pages. If you cannot pay any or all of these charges please let us know. GRS Society members receive a discounted rate of \$200 per page.
- 2) This pdf contains 2 proofs. The first half is the version that will appear on Xplore. The second half is the version that will appear in print. If you have any figures to print in color, they will be in color in both proofs.
- 3) The “Open Access” option for your article expires when the article is published on Xplore in an issue with page numbers. Articles in “Early Access” may be changed to Open Access. If you have not completed your electronic copyright form (ECF) and payment option please return to Scholar One “Transfer Center.” In the Transfer Center you will click on “Manuscripts with Decisions” link. You will see your article details and under the “Actions” column click “Transfer Copyright.” From the ECF it will direct you to the payment portal to select your payment options and then return to ECF for copyright submission.

AQ:1 = Please note that “viewing zenithal angle” has been changed to “viewing zenith angle” throughout the text for consistency.

AQ:2 = Please confirm or add details for any funding or financial support for the research of this article.

AQ:3 = Please confirm whether the edits made in the current affiliation of all the authors are correct.

AQ:4 = Please confirm the postal code for CNRS, Institut Pierre Simon Laplace, Université de Toulouse, and Laboratoire de Météorologie Dynamique.

AQ:5 = Please provide the expansions for SEVIRI and AMSU.

AQ:6 = Please check the sentence “The use of geophysical targets like ...” for clarity.

AQ:7 = Please check and confirm whether the edits made are appropriate: “Some studies on these geometric effects discussed the different configurations of cloud fields.”

AQ:8 = Please provide the organization name, organization location, and report no. for Refs. [11] and [12].

AQ:9 = Please provide the organization location and report no. for Ref. [19].

AQ:10 = Please provide the volume no. for Ref. [25].

AQ:11 = Please provide the organization name and organization location for Refs. [30] and [31].

AQ:12 = Please provide the year of completion when the author Rémy Roca received the M.S. degree.

AQ:13 = Please provide the year of completion when the author Sophie Cloché received the M.S. degree.

AQ:14 = Please provide the location for CETP.

# Homogenization of Geostationary Infrared Imager Channels for Cold Cloud Studies Using Megha-Tropiques/ScaRaB

Thomas Fiolleau<sup>1</sup>, Rémy Roca, Sophie Cloché, Dominique Bouniol, and Patrick Raberanto

**Abstract**—Infrared (IR) observations from the fleet of multi-agencies meteorological geostationary satellites have a great potential to support scientific and operational investigations at a quasi-global scale. In particular, such a data record, defined as the GEOring data set, is well suited to document the tropical convective systems life cycles by applying cloud tracking algorithms. Yet, this GEOring data set is far from being homogeneous, preventing the realization of its potential. A number of sources of inhomogeneities are identified ranging from spatiotemporal resolutions to spectral characteristics of the IR channels and calibration methodologies. While previous efforts have attempted to correct such issues, the adjustment of the cold part of the IR spectrum remains unfit for cold cloud studies. Here, a processing method is introduced to minimize the inhomogeneities against a reference observational data set from the Scanner for Radiation Budget (ScaRaB) instrument onboard the Megha-Tropiques satellite. The method relies on the collocations between the geostationary observations and the reference. The techniques exhibit significant sensitivity to the selection of the relevant pairs of observations requiring a dedicated filtering of the data. A second effort is then proposed to account for the limb-darkening effect and a method is developed to correct the brightness temperature (BT) dependence on the geostationary viewing zenith angle (VZA). Overall, results show a residual after the processing of 0 K between any of the geostationary data and the ScaRaB reference. The final calibrated and limb-adjusted IR observations are then homogeneous for cold BT lower than 240 K with a standard deviation lower than 1.5 K throughout the GEOring.

**Index Terms**— Calibration and spectral corrections, cold cloud studies, geostationary satellites, infrared (IR) image sensors, limb-darkening corrections.

## I. INTRODUCTION

METEOROLOGY agencies monitor individually operational geostationary platforms, which when used all together permit an observation for all longitudes of the Earth

Manuscript received July 17, 2019; revised November 25, 2019 and January 22, 2020; accepted February 4, 2020. (Corresponding author: Thomas Fiolleau.)

Thomas Fiolleau and Rémy Roca are with the Laboratoire d'Etudes en Géophysique et Océanographie Spatiales, CNRS, 31400 Toulouse, France (e-mail: thomas.fiolleau@legos.obs-mip.fr; remy.roca@legos.obs-mip.fr).

Sophie Cloché is with CNRS, Institut Pierre Simon Laplace, 75252 Paris, France (e-mail: sophie.bouffies-cloche@ipsl.fr).

Dominique Bouniol is with the Centre National de Recherches Météorologiques, CNRS, Météo-France, Université de Toulouse, 31057 Toulouse, France (e-mail: dominique.bouniol@meteo.fr).

Patrick Raberanto is with the Laboratoire de Météorologie Dynamique, CNRS, 75016 Paris, France (e-mail: patrick.raberanto@lmd.polytechnique.fr).

Color versions of one or more of the figures in this article are available online at <http://ieeexplore.ieee.org>.

Digital Object Identifier 10.1109/TGRS.2020.2978171

on a large latitudinal band ( $\sim 60^\circ$  S– $60^\circ$  N) with similar instruments. The potential benefit of such an observing capability has triggered numerous efforts in the past 40 years to make use of it for various applications, ranging from the elaboration of a unique perspective on clouds studies [1], [2] for precipitation estimation [3], climate studies [4], and global visualization applications [5]. Yet, when carefully examined, this GEOring appears to be far from a homogenous suite of instruments operated in a similar fashion. The space/time resolution and sampling differ across the platforms. The acquisition procedure also differs among the satellites (from South to North, North to South, or by sector). The calibration procedure of each instrument is also performed at the individual level with the instruments' specific modes of operation. Since 2011, for the infrared (IR) channels, the agencies provide alternative calibration coefficients obtained from a statistical comparison to hyperspectral IR measurements from low earth-orbiting satellites using the common methodology of the Global Space-Based InterCalibration System (GSICS) [6]. Nevertheless, the GSICS currently only provides calibration coefficients referenced to the NASA Earth Observing System (EOS), Aqua Atmospheric IR Sounder (AIRS), and the Exploitation of Meteorological Satellites (EUMETSAT)–Centre National d'Etudes Spatiales (CNES), Meteorological Operation (MetOp), and IR Atmospheric Sounding Interferometer (IASI) calibration standard. This harmonization effort does not take into account spectral band responses and viewing angle effects, which are needed for sensor homogenization. Indeed, while often referred to as a unique IR channel, the multiple instruments do show some spectral differences as well.

Most of the spectral imagers onboard geostationary satellites monitor with a relatively high temporal frequency the calibration coefficients for thermal IR channels by using onboard blackbody references. Some of the differences in the temperature measurements from one geostationary satellite to another can be explained by the differences in the calibration references, methods, as well as in the spectral filter functions. Moreover, it has been observed that the spectral imagers may degrade over time with different rates [7], [8]. The geostationary imagers can also be affected by short-term variations. The accumulation of ice on the surface of the imager optics modifies their spectral response function (SRF) and consequently affects the measurement of the temperatures. To face these issues, decontamination events are regularly applied to the radiometers inducing

TABLE I  
SUMMARY OF THE TECHNICAL CHARACTERISTICS OF THE VARIOUS EXISTING IR GEORING DATA SETS

Products	Spatial resolution	Temporal resolution	Spatial coverage	Temporal coverage	Calibration and temporal normalization	Limb darkening correction	Data source
Gridsat-B1	0.07°	180 min	70°S-70°N	1980-present	HIRS channel 8 [14]	Yes	ISCCP-B1
CPC	~ 0.04°	30 min	60°S-60°N	2000-present	No absolute calibration and no temporal normalization	Yes	Native
CLAUS	0.5°	180 min	Global*	1983-2006	ISCCP- B3	Yes	ISCCP-B3
CLAUS	0.3°	180 min	Global*	1985-2008	ISCCP- B3	Yes	ISCCP-B3
ISCCP-B1	Native FoV subsampled to ~ 0.1°	180 min	70°S-70°N	1980-present	AVHRR channel 5 [13]	No	Native
ISCCP-B3	Native FoV subsampled to ~ 0.3°	180 min	70°S-70°N	1983-2009	AVHRR channel 5 [13]	No	Native
This study	0.04°	30 min	35°S-35°N	2012-2016	SCARAB-IR channel 4	yes	Native

instability in the temperature measurements [9]. This effect has been particularly shown for the Meteosat Visible IR Imager (MVISIR) onboard the Meteosat-7 geostationary platform.

A diurnal cycle effect can also affect the imager calibration, especially for the instruments on the three-axis stabilized geostationary platforms [7], [9]. It has been shown that the sun-synchronous orbits of MetOp/IASI and EOS/AIRS used in the GSICS calibration are not sufficient to completely correct the diurnal IR calibration issues [10]. The precessing orbit of the tropical rainfall measuring mission (TRMM) platform and the observations of its visible and IR scanner (VIRS) have then been used to quantify and correct such a midnight IR calibration anomaly [10]. IR observations are also dependent on the geostationary viewing zenith angle (VZA). The issue is called limb darkening, corresponding to a decrease in the temperature as the VZA increases.

These multiple sources of inhomogeneity have prevented the full use of this unique observational capability, although a number of successful projects have attempted to overcome the above-listed limitations. Indeed, a number of significant efforts have been proposed in the last two decades to produce more or less homogeneous “global” archive of geostationary data sets for various applications. It ranges from cloud climatology computations (International Satellite Cloud Climatology Project (ISCCP)-B1, ISCCP-B3, and Cloud Archive User Service (CLAUS) [11]), hurricane trend analysis, support of precipitation estimation (Gridded Satellite (GridSat) [12]), real-time monitoring of precipitation (Climate Prediction Center (CPC) [13]), for the enhancement of radiation budget averages [8]. Additional information on these GEORing data sets is listed in [4]. Table I summarizes the available IR GEORing data sets altogether with their respective properties

and homogeneity levels. The ISCCP-B1 and B3 have been subsampled to a 180-min temporal resolution and to, respectively, ~0.1° and ~0.3° spatial resolution. They have been calibrated and spectrally normalized using advanced very high-resolution radiometer (AVHRR) observations [14]. The CLAUS data sets rely on the ISCCP-B3 and have been reprojected to an equal angle map projection with a spatial resolution of 0.3° and 0.5°. The GridSat-B1 is based on the ISCCP-B1 data set remapped to a 0.07° regular grid. In addition to the intercalibration used for the ISCCP data set, a second calibration using the high-resolution IR radiation sounder (HIRS) observations has been applied to correct a bias at cold temperatures observed after 2001. The CPC product is built in real time from native geostationary observations. The data are remapped to a regular grid of ~0.04° spatial resolution and are available every 30 min. To reduce the spectral differences and calibration issues, a complex, multistep, multiregional procedure is applied by comparing the brightness temperatures (BTs) from pairs of geostationary platforms. However, this procedure does not provide any absolute calibration. Also note that a limb correction has been performed on the GridSat-B1, CPC, and CLAUS data. In short, while a number of efforts have paved the way for a quantitative use of the GEORing data sets, no dedicated effort toward the cold BT regimes has been promoted so far. Yet, cold cloud studies benefit a lot from geostationary IR observations, for cloud microphysical or macrophysical parameters retrievals. The spatiotemporal resolution of the measurements further allows the life cycle analysis of the cold cloudiness and the estimation of related parameters. The present GEORing attempt is directed toward these scientific applications. In particular, it will serve as the input of the realization of a tropical mesoscale convective system data set using the TOOCAN algorithm [15].

TABLE II  
TECHNICAL CHARACTERISTICS OF THE OPERATIONAL GEOSTATIONARY SATELLITES FLEET AND THE ASSOCIATED IMAGERS USED OVER THE 2012–2016 PERIOD

Platform	Nadir location	Instrument	Central wavelength	Spectral interval	Spatial resolution at nadir	Temporal resolution	Region of interest	Source	Period
GOES-15	135° W	IMAGER	10.7 μm	10.2-11.2 μm	4 km	30 min	180° W-105° W 35° S-35° N	NOAA / DWD	Jan 2012- Dec 2016
GOES-13	75° W	IMAGER	10.7 μm	10.2-11.2 μm	4 km	30 min	111° W-30° W 35° S-35° N	NOAA / DWD	Jan 2012- Dec 2016
METEOSAT-8/9/10	0°	SEVIRI	10.8 μm	9.8-11.8 μm	3 km	15 min	45° W-45° E 35° S-35° N	EUMETSAT/ AERIS	Jan 2012- Dec 2016
METEOSAT-7 (IODC)	57.5° E	MVIRI	11.5 μm	10.5-12.5 μm	5 km	30 min	12° E-107° E 35° S-35° N	EUMETSAT/ AERIS	Jan 2012- Dec 2016
MTSAT-2	145° E	IMAGER	10.8 μm	10.3-11.3 μm	4 km	30 min	94° E-170° W 35° S-35° N	AERIS/ CIMSS	Jan 2012- May 2015
HIMAWARI-8	140.7° E	AHI	11.2 μm	11.0-11.4 μm	2 km	10 min	94° E-170° W 35° S-35° N	AERIS/ JMA	Jun 2015- Dec 2016

148 Such analyses require observations with a minimal temporal  
 149 resolution of 30 min [15], [16] to ensure tracked objects  
 150 overlap between two images. Such kind of studies requires the  
 151 use of thresholds applied to BT, ranging from 200 to 240 K,  
 152 depending upon the analysis [17], [15]. A homogeneous data  
 153 set is then mandatory, if one wants to proceed with the whole  
 154 tropical belt. The homogeneity and basic requirements for a  
 155 GEOring IR data set geared toward tropical cold cloud tracking  
 156 applications can be summarized as follows:

- 157 1) High-resolution spatial footprint and high spatial reso-  
 158 lution (~5 km).
- 159 2) A minimum of 30 min time sampling.
- 160 3) A spatial coverage dedicated to the tropics.
- 161 4) Homogenized BTs through spectral and calibration  
 162 adjustment.
- 163 5) Limb adjustment of IR observations.

164 Matching these requirements with the specifications of the  
 165 IR data sets summarized in Table I confirms the need for  
 166 a dedicated level 1c GEOring IR tailored for cold cloud  
 167 tracking applications. Moreover, the current implementation  
 168 of the GSICS coefficients computation is directed toward the  
 169 warm part of the spectrum [8], ruling out its use for cold  
 170 cloud studies calling for an alternative, cold cloud compliant,  
 171 absolute calibration reference for the GEOring. The limb  
 172 effect is less strong over the cold part of the temperature  
 173 spectrum than at the warm and clear sky end of the spectrum,  
 174 and the limb correction is easier to set up for cold cloudy  
 175 scenes (BTs < 240 K) than for the clear atmosphere. This

effect is strongly nonlinear and is thought to be impactful  
 only for the viewing angle above 26.5° [11]; it may still  
 require a correction for a homogeneous interpretation of the  
 BT field all through the image. It is difficult to establish  
 requirements once and for all in terms of residuals difference  
 in the homogeneous data, based on the radiometric noise of the  
 first generation sensors and the various sources of uncertainties  
 in the adjustment procedure and basic cloud-oriented retrievals  
 sensitivity. We propose to target a less than 1.5 K standard  
 deviation among any of the two geostationary satellites in the  
 final calibrated and limb-adjusted product for BTs < 240 K.

## 187 II. DATA

### 188 A. Five-Year Database of IR Geostationary Observations 189 Over the Entire Tropics

190 Thermal channel BT images obtained by the operational  
 191 meteorological geostationary satellite fleet are used over  
 192 the 35°S–35°N latitude belt and for the whole 2012–2016  
 193 period. Table II shows the geostationary IR data used to  
 194 cover the entire tropics for this period. The geostationary  
 195 data set has been collected from different sources: the U.S.  
 196 National Oceanic and Atmospheric Administration (NOAA),  
 197 the European Organization for the Exploitation of Meteorological Satellites (EUMETSAT), the Japan Meteorological Agency (JMA), and the French Atmosphere and Service Data Pole (AERIS). Note that the Multifunctional Transport Satellite (MTSAT) data set has also been completed from the Space Science and Engineering Center (SSEC) of the University of

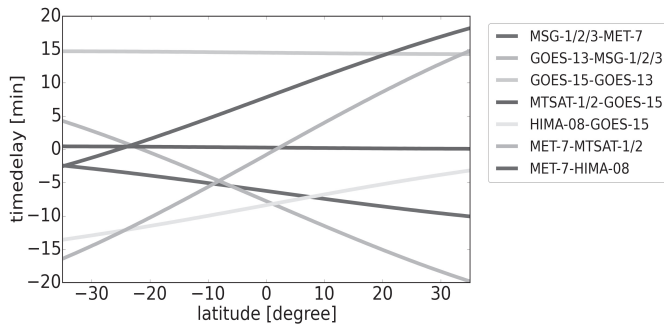


Fig. 1. Time delay of acquisition between pairs of geostationary images according to the latitude.

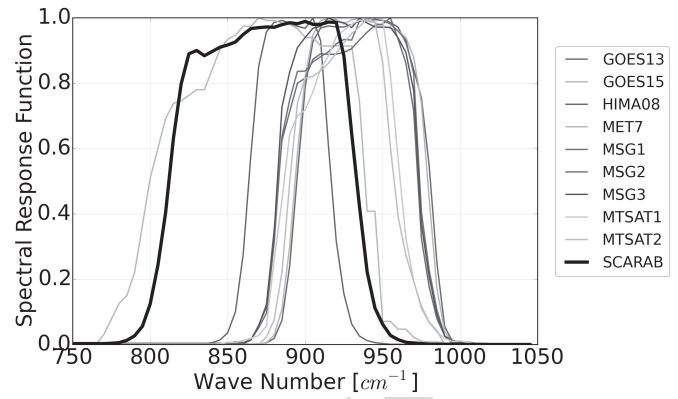


Fig. 2. SRF of the IR channel of the GEOring. The black line is the spectral response of the channel 4 of the ScaRaB instrument.

203 Wisconsin–Madison. The technical characteristics of each geo-  
 204 stationary platform and their imagers are described in Table II  
 205 and can differ from one platform to another. First, considering  
 206 the temporal resolution, Meteosat Second Generation (MSG)  
 207 and HIMAWARI-8 observe the Earth, respectively, with  
 208 a 15- and 10-min time resolution, while the other platforms  
 209 display a 30-min temporal resolution. Similarly, the scan-  
 210 times vary from 7 min for HIMAWARI-8 to 25 min for  
 211 Meteosat-7. The Geostationary Operational Environmental  
 212 Satellite (GOES)-13 and GOES-15 sensors follow a complex  
 213 scanning sector schedule. The full disk images are produced  
 214 every 3 h, while the northern hemisphere and the southern  
 215 hemisphere images are produced every 30 min with a time  
 216 lag of few minutes between each scan. Also, note that the  
 217 scanning schedule of MTSAT-2 does not provide half-hourly  
 218 sampling of the southern hemisphere region. Contrary to the  
 219 other imagers, the GOES-13 imager starts its earth scan at  
 220 15 and 45 min of the hour. Also note that Meteosat first-  
 221 and second-generation imagers start their earth scan from the  
 222 southeast corner, whereas NOAA and JMA platforms begin  
 223 their earth scan from the northwest corner. All these tempo-  
 224 ral scanning differences imply some time delays between  
 225 neighboring platforms observing the same region (Fig. 1).  
 226 While the 15-min time delay is constant for the pairs of the  
 227 GOES-15/GOES-13 and MTSAT-2/GOES-15 platforms, the  
 228 time delay varies according to the latitude for the other pairs  
 229 of geostationary platforms. At 35° S, a maximum time delay  
 230 is found for the pair of MSG/GOES-13 platform of around  
 231 20 min. The maximum time delay amplitude accounted for the  
 232 pair of the Meteosat-7/MTSAT-2 platforms and varies between  
 233 –16 and 15 min.

234 Depending on the considered satellite, spatial resolution at  
 235 nadir differs from one geostationary satellite to another and  
 236 ranges from 2 km for HIMAWARI-8 to 5 km for Meteosat-7.  
 237 In addition to the resolutions disparities, the GEOring is also  
 238 characterized by differences in the central wavelength and the  
 239 associated SRFs of each of the instruments (Fig. 2). While  
 240 the central wavelength ranges between 10.7 and 11.5  $\mu\text{m}$  for  
 241 the GOES imagers and the Meteosat-7 imager, respectively,  
 242 two types of SRFs can define the IR channels. The GOES-13,  
 243 GOES-15, MTSAT-2, and HIMAWARI-8 imagers display nar-  
 244 rowband channels with a bandwidth lower than 1  $\mu\text{m}$ , whereas  
 245 the Meteosat-7/MVIRI and MSG/SEVIRI imagers exhibit

broader channels characterized by a 2  $\mu\text{m}$  bandwidth. A broad-  
 band channel is highly sensitive to ice contamination on the  
 optics of the imagers, modifying their SRFs, and consequently,  
 introducing a calibration error. Operational decontamination  
 procedures are applied regularly to remove the ice build-up  
 on the optics. Thus, spectral differences, as well as the  
 individual satellite calibration procedures, contribute to the  
 GEOring radiometric inhomogeneities.

### B. Megha-Tropiques/ScaRaB-3 Observations

The Scanner for Radiation Budget (ScaRaB) instrument  
 on the Megha-Tropiques platform [18] is the third of its  
 kind [19], [20] and has been designed to measure the Earth  
 radiation components at the top of the atmosphere with high  
 accuracy (<1%). The instrument acquires data across the  
 satellite track with a swath of  $\sim 2200$  km from 30° S to 30° N.  
 It is a broadband radiometer with four channels. The total  
 channel measures the total energy between 0.2 and 100  $\mu\text{m}$ .  
 The shortwave channel (0.2–4  $\mu\text{m}$ ) is subtracted from the total  
 channel to obtain the longwave part of the spectrum [21]. The  
 fourth channel is an IR thermal channel (10.5–12.5  $\mu\text{m}$ ) which  
 is used in this article (Fig. 2). The instrument operates nom-  
 inally since the beginning of the mission and its operational  
 performances are well in line with the specifications [22]–[24].  
 The nominal resolution of the ScaRaB footprint at nadir is  
 40 km and is detailed in [18].

The stability of the instrument is monitored by the CNES  
 on a daily basis and so far, the Megha-Tropiques instruments  
 have shown remarkable stability [25]. The use of geophysical  
 targets like deep convective clouds (DCC) has been shown  
 to be useful for geophysical calibration and cross-calibration  
 of either broad radiometers [26], [27]. It is used here to  
 showcase the relative stability of the channel 4 to that of  
 the longwave channel. Fig. 3 shows the ratio between the  
 radiance in channel 4 and channel 1 over the studied period  
 for various deep convective regimes. The two channels of the  
 instrument show no sign of relative degradation and a very  
 steady behavior. Comparisons with the Clouds and the Earth's  
 Radiant Energy System (CERES) instrument using dedicated  
 collocation campaigns [28] further indicate a very good agree-  
 ment between the two instruments' longwave channels [29].

246  
247  
248  
249  
250  
251  
252  
253  
254  
255  
256  
257  
258  
259  
260  
261  
262  
263  
264  
265  
266  
267  
268  
269  
270  
271  
272  
273  
274  
275  
276  
277  
278  
279  
280  
281  
282  
283  
284  
285

AQ:6

285

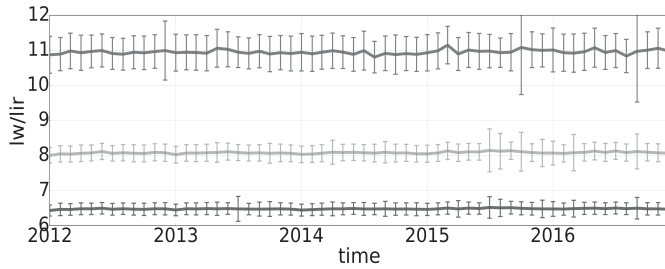


Fig. 3. Evolution of the ratio between measured radiance in the longwave band and in the IR channel of ScaRaB over the 2012–2016 period for various deep convective regimes. The blue curve corresponds to an IR radiance lower than  $2.25 \text{ W} \cdot \text{m}^{-2} \cdot \text{sr}^{-1}$  corresponding to a 187 K BT, the yellow one lower than  $4.25 \text{ W} \cdot \text{m}^{-2} \cdot \text{sr}^{-1}$  (207.4 K), and the red curve corresponds to an IR radiance lower than  $7.75 \text{ W} \cdot \text{m}^{-2} \cdot \text{sr}^{-1}$  (224.5 K).

286 The ScaRaB instrument is also thermally controlled and is not  
 287 impacted by icing events as shown in the monitoring of the  
 288 instrument performances [22], [23]. The combination of an  
 289 accurate and stable instrument makes it a well-suited reference  
 290 to adjust the geostationary data.

291 Here we use the so-called level 2B products that consist  
 292 of a  $0.5^\circ$  regularly gridded instantaneous directional radiances  
 293 ( $\text{W} \cdot \text{m}^{-2} \cdot \text{sr}^{-1}$ ). The original measurements are averaged on the  
 294 regular grid using a statistical technique and the point spread  
 295 function of the instrument [30]. Since 2011, the availability  
 296 of this product is about 99.9%, making it a useful resource as  
 297 a reference instrument for the spectral homogenization of the  
 298 GEORing data. Note that unlike sun-synchronous platforms,  
 299 the precessing orbit of Megha-Tropiques samples all the local  
 300 times every 51 days allowing the collocation with the geo-  
 301 stationary data all through the day and then the correction of  
 302 the midnight IR anomaly [10], [18], [31]. The low inclination  
 303 at the equator ( $20^\circ$ ) and high altitude of flight (865 km) also  
 304 allow high repetitive measurements in the tropics [18].

### 305 III. HOMOGENOUS LEVEL 1C IR DATA SET 306 FOR THE TROPICS FOR 2012–2016

#### 307 A. Homogenization of the Temporal Resolution

308 Given the requirements for cold cloud studies (see  
 309 Section I), the lack of temporal resolution homogeneity  
 310 between the geostationary imagers is accounted for by using  
 311 a 30-min temporal frequency for all the platforms, preventing  
 312 the use of MTSAT data in the southern hemisphere.

#### 313 B. Homogenization of the Spatial Resolution

314 A common equal angle grid of  $0.04^\circ \times 0.04^\circ$  has been  
 315 selected for all the platforms to account for this source of  
 316 inhomogeneity. This resolution is very close to the native  
 317 resolution of GOES-13, GOES-15, MTSAT-2, and Meteosat-7  
 318 data. The regridding process is performed by applying the  
 319 inverse distance weighting method in the radiance space with  
 320 a maximum search radius corresponding to the sum of half  
 321 of the geostationary spatial resolution for a given pixel plus  
 322 a half of the equal angle grid resolution. Then, the average  
 323 radiance is transformed in BT using the Planck function in  
 324 order to account for its nonlinearity.

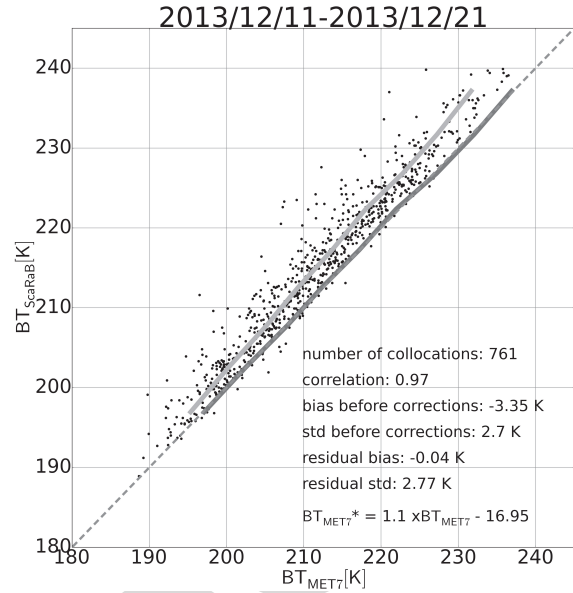


Fig. 4. Scatter plot between  $\text{BT}_{\text{MET7}}$  and  $\text{BT}_{\text{ScaRaB}}$  obtained after the filtering procedure over a ten-day period starting in 2013/12/11 for BT in the range [180–240 K]. The orange line corresponds to the average BT for each 5 K bin. The blue line corresponds to the residual bias.

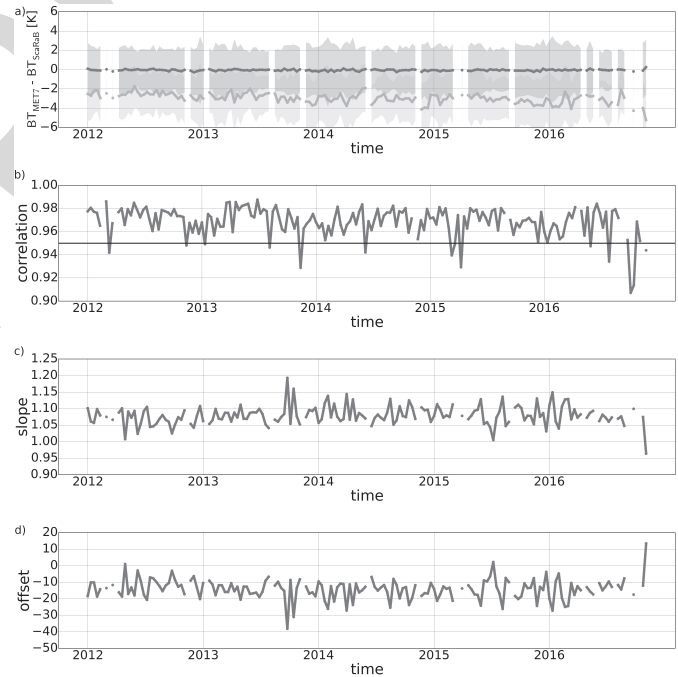


Fig. 5. (a) Time series of decadal initial BT bias (orange) and corrected BT bias (blue) for Meteosat-7 IR observations with respect to ScaRaB in the range [180–240 K]. The filled and transparent areas in orange and blue represent the standard deviations; (b) Time series of decadal linear regression correlations, (c) slope, and (d) offset between the ScaRaB and the Meteosat-7 IR observations in the range [180–240 K].

#### 325 C. Intercalibration and Spectral Normalization

326 1) *Regression Technique:* The use of a common low  
 327 earth-orbiting satellite, carrying an IR radiometer to anchor  
 328 each of the platforms to a common reference data set, forms  
 329 the basis of the different intercalibration and normalization  
 330

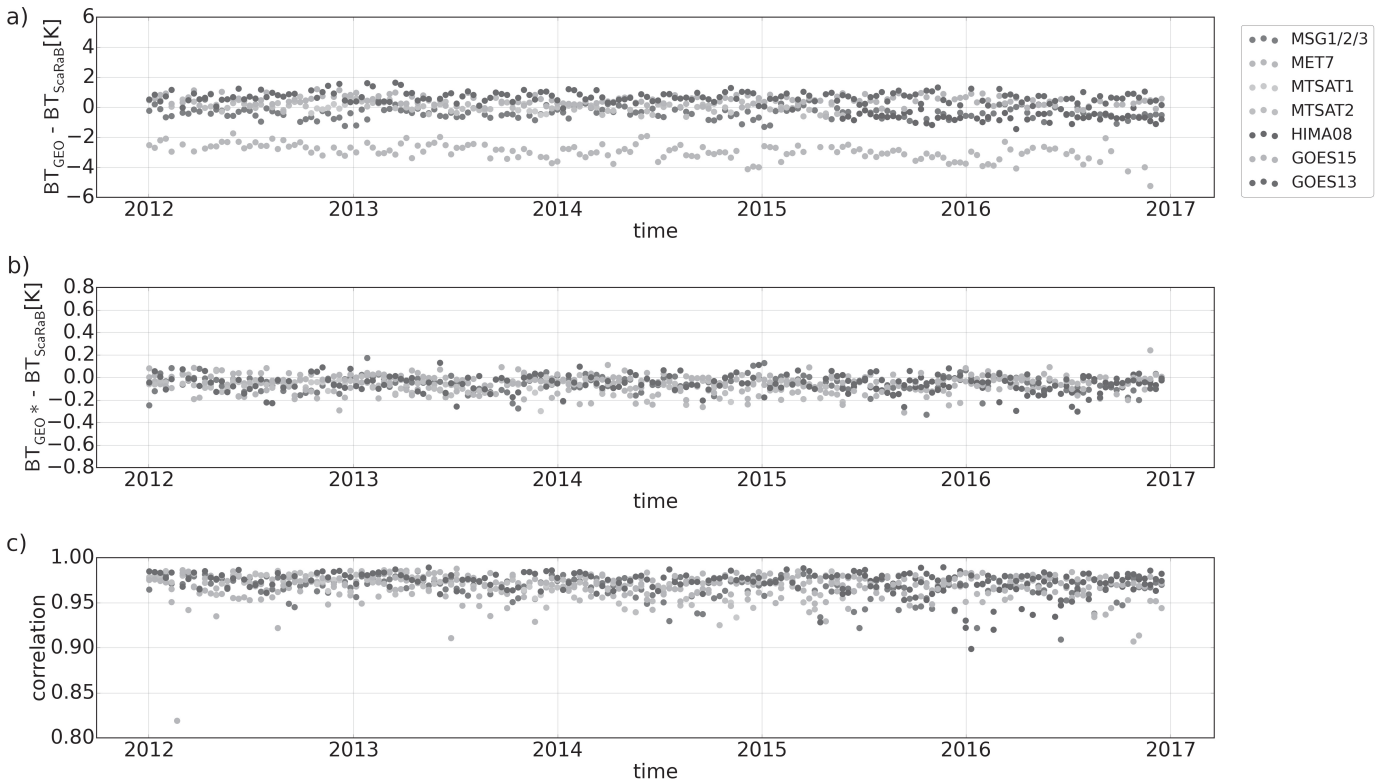


Fig. 6. (a) Time series of initial BT bias of geostationary IR observations with respect to ScaRaB in the range [180–240 K]. (b) Time series of BT bias between the geostationary IR observations and the ScaRaB observations in the range [180–240 K] after spectral and calibration corrections. (c) Time series of correlations between the ScaRaB and the geostationary IR observations in the range [180–240 K]. Each dot corresponds to a ten-day period.

330 efforts listed in Table I [14], [32] or under the GSICS  
 331 calibration procedure [7]. Regression-based techniques are  
 332 the most commonly used approaches. The difficulty arises in  
 333 building the pairs (space/time/angular collocation) as well as  
 334 in selecting the pairs of observations that will be regressed.  
 335 This selection can have a strong impact on the result. Hence,  
 336 it has been noted that the original ISCCP intercalibration was  
 337 skewed toward a warm scene due to the implementation of  
 338 the pairs selection filter prior to the regression computation,  
 339 yielding a  $\sim 4$  K cold bias on the cold part of the spectrum [33].  
 340 Similarly, most of the tropical observations are located over  
 341 large BT values and only a few of them are explained by  
 342 DCCs. As the larger population of collocations is explained  
 343 by high BT, the GSICS corrections are optimized for clear  
 344 sky conditions and are not well suited for the cold cloud  
 345 scenes [7]. A specific homogenization of the IR geostationary  
 346 database is then required to fit with the objective of cold  
 347 cloud tracking applications. This homogenization consists of  
 348 a spectral normalization as well as an intercalibration of the  
 349 various geostationary imagers focused on high cold clouds and  
 350 on cold BTs. For this purpose, the BTs from the geostationary  
 351 imagers are calibrated and spectrally normalized against the  
 352 ScaRaB channel 4 measurements. The final data set then  
 353 consists of a 10.5–12.5  $\mu\text{m}$  IR equivalent BT. Calibration  
 354 uncertainty is expected to be within 1 K, which is the typical  
 355 error for operational satellite calibration [34]. Contrary to  
 356 other geostationary imagers, the correction of the Meteosat-7/  
 357 MVIRI imager is restricted to an intercalibration procedure,

358 since its broad SRF is similar to the ScaRaB/channel 4 and  
 359 both of them are centered on 11.5  $\mu\text{m}$ .

360 2) *Selection of the Data Match-Ups for the Regression:* The  
 361 IR geostationary data from all the platforms are first remapped  
 362 from their native formats to a regular lon/lat 0.5° grid every  
 363 30 min to allow direct comparison with the ScaRaB/L2B data.  
 364 Prior to computing the averaged radiance and the associated  
 365 spatial standard deviation for each 0.5° grid point, the BTs of  
 366 each geostationary platform are converted in radiances ( $\text{mW} \cdot$   
 367  $\text{m}^{-2} \cdot \text{sr}^{-1} \cdot \text{cm}^{-1}$ ) by applying the Planck function. The information  
 368 on geostationary scan-time is also indicated for every grid  
 369 point. The collocation between the ScaRaB-L2B observation  
 370 and the IR 0.5°  $\times$  0.5° gridded geostationary data is reached  
 371 when both view the same scene with a predefined time delay  
 372 and similar viewing geometry. The predefined criteria are.

- 373 1) A maximum VZA of 20° and 26°, respectively, for the  
 374 ScaRaB and the geostationary observation, to ensure  
 375 alignment of the collocated pixels in viewing geometry  
 376 and to avoid limb-darkening issues [35].
- 377 2) A maximum time delay of 10 min between two col-  
 378 located pixels, which is a tradeoff between a relevant  
 379 number of match-ups to populate the decadal regressions  
 380 and the best possible temporal precision.
- 381 3) The IR-gridded radiances are regressed in units of  
 382 temperature.

383 As we focus on high cold clouds scenes, we have developed  
 384 a filtering procedure that keeps more collocation scenes at a  
 385 colder temperature. Indeed, a bulk of collocations occurs at

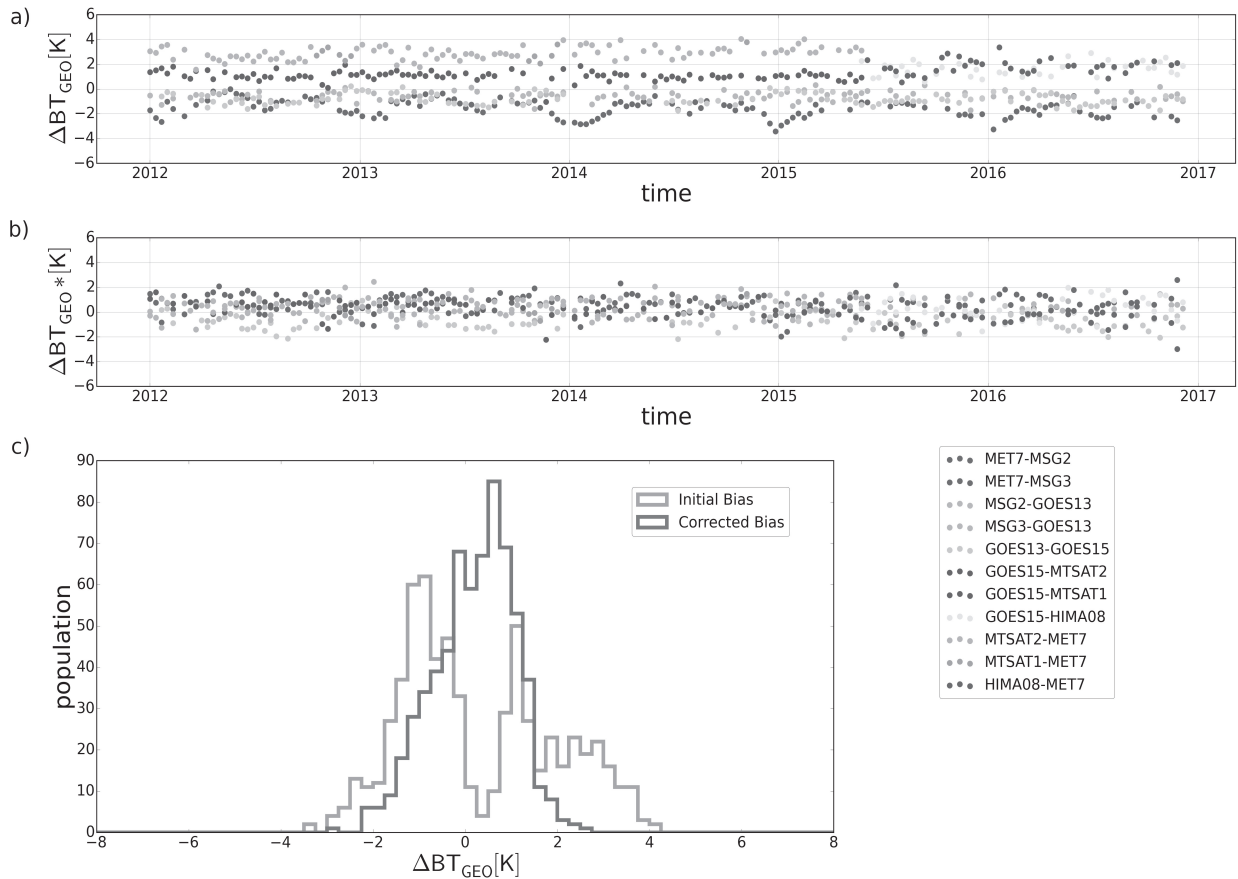


Fig. 7. (a) Time series of initial BT bias between pairs of geostationary platforms observing common areas with an equivalent VZA in the range [180–240 K]. (b) After spectral and calibration corrections; each dot corresponds to a ten-day period. (c) Distribution of the bias before and after corrections over the 2012–2016 period for all the pairs of geostationary platforms for all the ten-day periods.

386 a warmer temperature and displays a lower standard deviation [33]. To separate the high cold cloud population from  
 387 the warmer targets in the scatterplot, thresholds are applied  
 388 to the GEO standard deviation that depends on the BT.  
 389 Pixels presenting a  $BT_{GEO} > 240$  K are rejected if their  
 390 standard deviations are larger than 0.5 K and pixels with  
 391  $BT_{GEO} < 240$  K are kept if their standard deviations are  
 392 lower than 2 K. Besides separating the high cold cloud popu-  
 393 lation from clear sky pixels, this filtering procedure ensures  
 394 that heterogeneous moving objects do not contaminate the  
 395 collocation scenes and that the two instruments observe the  
 396 same high cloud target. Assuming also that the IR radiometers  
 397 onboard geostationary platforms have a linear response when  
 398 observing high cold cloud homogeneous scenes [8], [36], the  
 399 calibration and spectral normalization corrections are then  
 400 based on linear regressions computed over a 180–240 K  
 401 range. For this, the collocated  $BT_{GEO}$  and  $BT_{ScaRaB}$  are binned  
 402 and averaged for every  $BT_{ScaRaB}$  interval of 5 K from 180 to  
 403 240 K. The regression coefficients are then computed over  
 404 these binned data every ten days and over a ten-day period.  
 405 This is required to ensure statistical robustness but prevent  
 406 higher frequency variation (<10 days) of the calibration  
 407 issues (due to decontamination for instance) to be accounted  
 408 for. As shown below, such higher frequency effects do not  
 409 impact the residuals of the regression. Correlations are used to

determine the ten-day period that might have match-ups errors.  
 If the correlations are lower than 0.95 or if the population  
 of collocations does not exceed ten matchups, we consider  
 that the linear regression cannot be computed and that every  
 ten-day period is removed from our analysis. In this case,  
 the previous regression coefficients are replicated.

3) *Results:* Fig. 4 shows an example of such a regression  
 computed from 761 collocated pixels between the Meteosat-7/  
 MVIRI imager and the Megha-Tropiques/ScaRaB observations  
 acquired over a ten-day period from 2013/2012/2011 and  
 for a range between 180 and 240 K. The  $11.5 \mu m$  channel  
 of Meteosat-7 exhibits a large negative bias ( $-3.35$  K) for  
 this considered BT and for this specific period. The blue  
 line shows the regression fit given by a slope of 1.11 and  
 an offset of  $-16.95$  K. The correction has produced a very  
 low residual bias, which averages at  $-0.04$  K over this  
 decadal period, and the correlation higher than 0.97 between  
 the two data sets shows the high quality of the regression  
 computation. Fig. 5(a) shows the time series of difference  
 between Meteosat-7/MVIRI and ScaRaB before and after  
 calibration over the 2012–2016 period. The Meteosat-7 BT  
 is corrected every ten days using the slopes and offset com-  
 puted from the linear regression. Over the period and for  
 the specific Meteosat-7 geostationary platform, 12% of the  
 decadal scatterplots are excluded from our analysis following

411  
412  
413  
414  
415  
416  
417  
418  
419  
420  
421  
422  
423  
424  
425  
426  
427  
428  
429  
430  
431  
432  
433  
434  
435

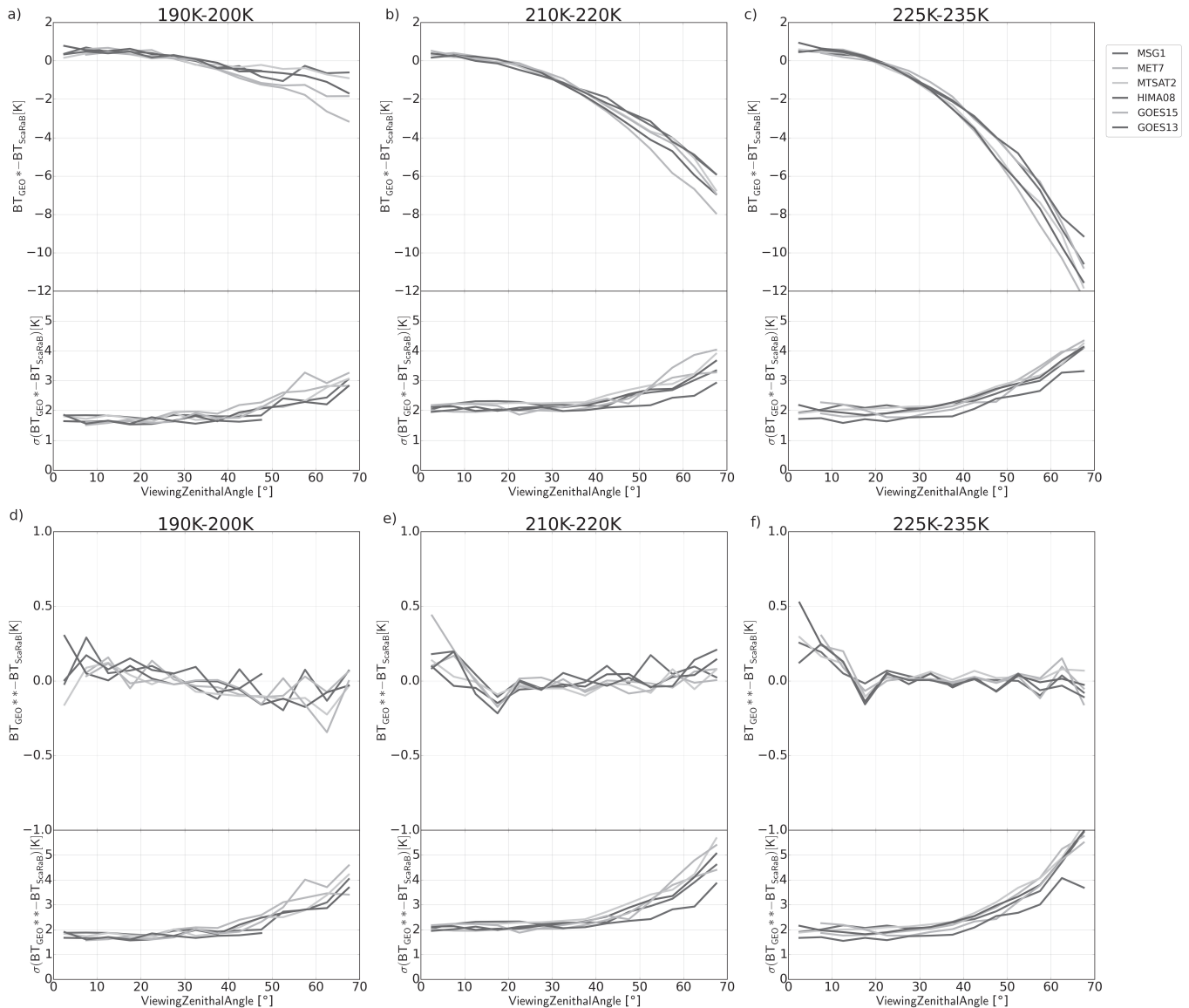


Fig. 8. Variation of the BT bias and the corresponding standard deviation between the GEO and the SCARAB observations according to the geostationary VZA, for a  $VZA_{ScaRaB} < 20^\circ$  and for three different ranges of  $BT_{ScaRaB}$ . (a)–(c) Before VZA corrections. (d)–(f) After VZA corrections.

the filtering procedure [Fig. 5(b)] and 87 405 collocations have then been used to compute the decadal regressions. One can observe that over the 2012–2016 period, and before the corrections, the Meteosat-7/MVIRI exhibits a negative bias, averaging at  $-2.98$  K and negatively increasing slightly with time due to contamination on the optics. This radiometric issue has been fully documented in [7]. The variations of the slopes and offsets are relatively stable over the period [Fig. 5(c) and (d)], showing the robustness of the methodology. After applying the calibration correction, the residual bias is very smooth, stable, and close to zero over the whole period. The calibration and spectral normalization corrections are applied on all the geostationary platforms available over the 2012–2016 period. The results have been obtained over the entire period, and for all the geostationary platforms by filtering 8% of the decadal scatterplots which did not pass our

quality control [Fig. 6(c)], leading to a comparison of around 655 000 collocations. Fig. 6(a) shows the time series of the decadal initial bias in BT for all the geostationary imagers with respect to the ScaRaB observations in the range 180–240 K. Over the 2012–2016 period, the Meteosat-7/MVIRI exhibits the highest error as discussed previously. It is also to be noted that the MSG/SEVIRI imager shows a relatively high negative bias ( $-1.39$  K) to be compared to the other instruments whose biases are mainly in the range  $-0.5$ – $0.5$  K over the entire period. While the calibration issues only explain the bias between Meteosat-7 and ScaRaB, the differences of temperature between ScaRaB and the other geostationary platforms can be explained by both a poor calibration and some differences in the SRF. The results of the intercalibration and spectral normalization are shown in Fig. 6(b). Over the entire period and for all the geostationary platforms, the decadal

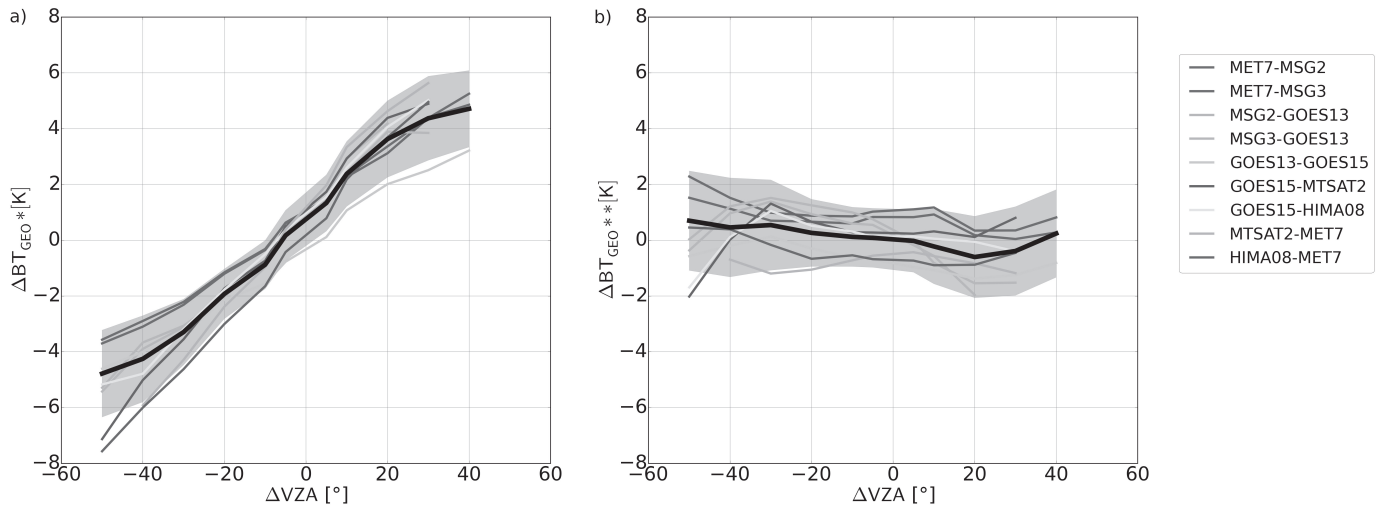


Fig. 9. Variation of the BT bias according to the VZA differences between pairs of geostationary platforms observing common areas and for  $BT_{ScaRaB}$  in the range [180–235 K]. (a) Before VZA corrections. (b) After VZA corrections. The BT bias and its standard deviation for all the pairs of geostationary platforms are represented respectively by the black line and the filled area in gray over the 2012–2016 period for all the ten days.

468 residual bias indicates a very low and stable bias, around 0 K,  
 469 with a standard deviation lower than 0.08 K between  $BT_{ScaRaB}$   
 470 and  $BT_{GEO}$ . The corrections are then directly applied to the  
 471 original geostationary data.

472 To fully describe the impact of the ScaRaB calibration  
 473 and spectral corrections, an independent validation has been  
 474 developed. The bias of uncorrected and corrected  $BT_{GEO}$  is  
 475 then computed in the range of 180–240 K every ten days  
 476 between pairs of neighbored geostationary platforms observing  
 477 common areas and sharing an equivalent VZA (Fig. 7). Indeed,  
 478 for two adjacent geostationary satellites, the BT bias at the  
 479 middle of the overlap region should average to zero, due to  
 480 the similar geometry for both platforms. Fig. 7(a) shows the  
 481 time series of decadal mean differences between uncorrected  
 482 BTs of each pair of geostationary satellites. Each color  
 483 represents a pair of geostationary platforms. Results indicate  
 484 a scatter of the decadal bias between  $-4$  and  $4$  K. The  
 485 maximum bias occurs for the BT differences between  
 486 MTSAT-1/2 and Meteosat-7, which averages at  $2.9$  K from  
 487 the beginning of 2012 to June 2015. The bias between  
 488 uncorrected  $BT_{MET-7}$  and  $BT_{MSG-1/2/3}$  exhibits a relatively  
 489 high bias ( $-1.62$  K on average) and is distinguishable from  
 490 the other pairs of geostationary satellites, in contrast to  
 491 its relatively high seasonal variations. The distribution of  
 492 the decadal initial bias for all the geostationary platforms  
 493 over the 2012–2016 period [Fig. 7(c)] reveals a multimodal  
 494 distribution, which averages at  $0.25$  K and displays a standard  
 495 deviation of  $1.65$  K. Fig. 7(b) shows that the corrections  
 496 applied to the geostationary IR observations improve the error  
 497 as well as the disparity of the scatter plot over the whole  
 498 period and for all the geostationary platforms. These results  
 499 are confirmed by the Gaussian distribution of the decadal  
 500 bias for corrected  $BT_{GEO}$  shown in Fig. 7(c), which averages  
 501 at  $0.19$  K with a standard deviation of  $0.87$  K. The resulting  
 502 geostationary satellite calibration residuals specifications are  
 503 hence well within the  $1$  K limit previously mentioned and

demonstrate the importance to develop a correction procedure  
 for the geostationary IR observations at cold temperatures.

#### D. Limb-Darkening Adjustment

504  
 505  
 506  
 507  
 508  
 509  
 510  
 511  
 512  
 513  
 514  
 515  
 516  
 517  
 518  
 519 AQ:7  
 520  
 521  
 522  
 523  
 524  
 525  
 526  
 527  
 528  
 529  
 530  
 531  
 532  
 533  
 534  
 535  
 536  
 537

1) *Methodological Considerations:* To complete the homogenization procedure of the geostationary database, we focus now on the dependence of the  $BT_{GEO}$  on the VZA. This issue, also called limb darkening, corresponds to a decrease in the temperature as the VZA increases. The greater optical path length of the absorbing atmosphere, as the VZA increases, results in a larger atmospheric absorption. Indeed, a longer optical path length contains much more water vapor and ozone explaining the observation of colder temperatures [35], [37], [38]. Cloudy scenes imply a second mechanism in the VZA issues [35]. A geometric effect may also be involved when the sides of the clouds obstruct the Earth's emitted radiation at a large VZA. Some studies on these geometric effects discussed the different configurations of cloud fields [39]. To prevent an erroneous analysis between meteorological situations, which occurred at nadir and at a large VZA, the BTs have to be limb-adjusted. Some studies have been carried out to limb adjust the IR observations for cloudy regions by establishing empirical limb correction functions, depending on the cosine of zenith angle from the radiative transfer model for low earth orbit platforms [39] and IR geostationary observations [40]. However, it has been shown [41] that the corrections developed by [39] underestimate the observed BTs. The variation of the radiance, according to the zenith angle, is approximated in the CLAUS data set, by applying a function of the cosine of the zenith angle. Another way to face the limb-darkening issues is to use observations from low earth orbit platforms. Limb-correction algorithms have been developed for microwave observations from the AMSU-A and are based on a physical-statistical methodology [37]. The limb-darkening problem has also been



544 the  $BT_{\text{GEO}}$  as a function of VZA is applied to  $BT_{\text{GEO}}$  only  
 545 for observations in the tropics. For mid-latitude regions,  
 546 an additional correction is applied to tackle the latitudinal  
 547 and seasonal dependence of  $BT_{\text{GEO}}$ . This dependence is  
 548 explained by a smaller contrast between the cloud top and  
 549 the Earth's surface in mid-latitudes than over the tropics.  
 550 This limb-darkening correction is used in GridSat and ISCCP  
 551 data sets [4]. However, this methodology is likely to suffer  
 552 from limitations to be used to homogeneously limb adjust a  
 553 fleet of geostationary satellites. Indeed, the limb adjustment,  
 554 developed in the 2000s and empirically derived from a  
 555 combination of a specific and limited set of instruments,  
 556 may also be biased for other and new generation of  
 557 geostationary instruments [12]. Moreover, the computation of  
 558 the limb-darkening correction is limited by the range of VZA,  
 559 due to the combination of the fixed location of geostationary  
 560 satellites inducing few observations of cold  $BT_{\text{GEO}}$ .

561 It appears important, for this article, to tackle limb-  
 562 darkening issues on geostationary satellite per geostationary  
 563 satellite over the full time period by using a common reference,  
 564 such as the IR observation from the ScaRaB instrument.  
 565 This correction focuses on cold clouds monitored by the IR  
 566 imagery of geostationary satellites previously intercalibrated  
 567 and normalized into a  $10.5\text{--}12.5\ \mu\text{m}$  IR equivalent BT, called  
 568  $BT_{\text{GEO}}^*$ . For this purpose, we perform for each GEO platform  
 569 a collocation procedure between the regular lon/lat  $0.5^\circ$  and  
 570 corrected IR geostationary data, presented previously, and the  
 571 ScaRaB/L2B IR observation over the entire 2012–2016 period.  
 572 The collocation procedure is applied under some criteria.  
 573 Where the zenithal angles of ScaRaB do not exceed  $20^\circ$ ,  
 574 the geostationary zenith angles can range from  $0^\circ$  to  $70^\circ$ . The  
 575 collocation is also performed with a time delay of less than  
 576 10 min between the GEO and the ScaRaB observations and for  
 577  $BT_{\text{ScaRaB}}$ , which does not exceed 235 K for standard deviations  
 578 lower than 2 K.

579 GEO-ScaRaB match-ups are binned into geostationary  
 580 zenith angle intervals of  $2^\circ$  and for zenith angles ranging  
 581 from  $20^\circ$  to  $70^\circ$ . For GEO VZAs lower than  $20^\circ$ , a unique  
 582 limb correction is performed. Moreover, to ensure a relevant  
 583 sample size on each  $2^\circ$  zenith angle bin, the regressions are  
 584 applied annually. For each zenith angle interval, the collocated  
 585  $BT_{\text{GEO}}^*$  and  $BT_{\text{ScaRaB}}$  are binned and averaged for every  
 586  $BT_{\text{ScaRaB}}$  interval of 5 K, from 180 to 235 K. To filter corrupted  
 587 collocated points, the binning procedure is performed when  
 588 at least ten samples are present. The limb correction then  
 589 consists of applying annual regressions between the binned  
 590 GEO and ScaRaB data for every  $2^\circ$  zenith angle bin and  
 591 for each geostationary platform. A second-order polynomial  
 592 regression has been preferred over the linear regression, due  
 593 to slight improvements in the minimization of the residuals.

594 2) *Results*: Fig. 8(a)–(c) shows the variation of the initial  
 595 bias between each GEO platform and ScaRaB, according  
 596 to the VZA for different bins of ScaRaB temperatures and  
 597 over the 2012–2016 period. First, one can observe a negative  
 598 increase in the bias as the VZA increases, whatever the range  
 599 of BT. For VZA lower than  $30^\circ$ , the absolute bias seems to be  
 600 lower than 1 K, whatever the  $BT_{\text{ScaRaB}}$  is. However, we can  
 601 observe drastic differences in the bias evolution depending on

the  $BT_{\text{ScaRaB}}$  bin. Indeed, at warmer  $BT_{\text{ScaRaB}}$  [225–235 K],  
 the negative increase in the bias according to the VZA is more  
 pronounced than for colder values of  $BT_{\text{ScaRaB}}$  [190–200 K].  
 For a VZA at  $40^\circ$ , the bias averages at  $-0.63$  K for  $BT_{\text{ScaRaB}}$ ,  
 ranging from 190 to 200 K and for all the GEO platforms,  
 while the bias averages at  $-2.9$  K for  $BT_{\text{ScaRaB}}$  greater than  
 225 K and for a similar VZA. It is also to be noticed that  
 the disparity of the bias among GEO platforms increases with  
 the VZA. Thus, at a  $60^\circ$  zenith angle and for the 225–235 K  
 range, the bias varies from  $-7.4$  to  $-9.5$  K for GOES-15 and  
 Meteosat-7, respectively. Such large errors have been previ-  
 ously reported for an older Meteosat first-generation satellite  
 (Meteosat-4) compared to NOAA/AVHRR reference [27].  
 Note that the uncertainty does not increase much with the BT  
 but increases with the VZA. Fig. 8(d)–(f) shows the results  
 of the limb-darkening corrections according to the variation  
 of the zenith angle for all the geostationary platforms and for  
 different ranges of  $BT_{\text{ScaRaB}}$ . Over the whole range of ScaRaB  
 BTs, the residual biases average at 0 K, regardless of the  
 geostationary platform and the zenith angles. These results  
 demonstrate the capability of the limb-darkening correction  
 methodology we have developed. An independent validation  
 is provided in Fig. 9 by comparing pairs of geostationary  
 platform observations. It shows the variation of the decadal  
 biases of  $BT_{\text{GEO}}^*$  between pairs of geostationary satellites,  
 according to the difference of their VZAs ( $\Delta VZA$ ), before  
 and after applying limb-darkening corrections. A  $\Delta VZA$  of  
 $0^\circ$  means that two adjacent geostationary platforms observe  
 the same region with an equivalent VZA. On the contrary,  
 a large  $\Delta VZA$  indicates that a given geostationary platform  
 observes a region with a nadir zenith angle, while the adjacent  
 geostationary platform monitors the same region with a limb  
 zenith angle. Before applying the zenith angle corrections,  
 we can observe an increase of  $BT_{\text{GEO}}^*$  bias for all the  
 platforms from  $\sim -5$  to  $\sim 5$  K as the  $\Delta VZA$  moves from  
 $-50^\circ$  to  $40^\circ$  [Fig. 9(a)]. The standard deviation, on its side,  
 varies between 0.86 K for a low  $\Delta VZA$  and 1.57 K for  
 large  $\Delta VZA$ . Results indeed indicate a larger disparity of  
 the  $BT_{\text{GEO}}^*$  biases between pairs of geostationary satellites  
 for large  $\Delta VZA$ . After applying the zenith angle correction  
 [Fig. 9(b)], the  $BT_{\text{GEO}}^{**}$  bias is relatively stable and averages  
 at 0.09 K with a standard variation of 1.43 K, regardless of  
 the variation of  $\Delta VZA$ . The standard deviation varies from  
 1.05 to 1.78 K for low and large  $\Delta VZA$ , respectively. Note  
 that when the limb-darkening issue is clearly improved and  
 corrected, the standard deviation for a low VZA is a little  
 larger than before applying the VZA correction.

#### IV. DISCUSSION AND CONCLUSION

In summary, a level 1c IR GEOing data set is introduced.  
 This data set is a consistent  $10.5\text{--}12.5\ \mu\text{m}$  IR equivalent BT  
 data set, with a homogeneous recalibration, a  $0.04^\circ \times 0.04^\circ$   
 spatial resolution, a 30 min common time resolution, and a  
 correction for limb effect. The data set covers the 2012–2016  
 period. The global homogeneity of the IR GEOing data set,  
 regardless of the variation of VZA, is then characterized by a  
 standard deviation of 1.43 K within any of two geostationary  
 satellites.

As discussed in the Introduction section, global geostationary IR observations provide useful resources to carry out studies on convective systems. Cold cloud tracking algorithms usually delineate cold clusters by applying a 235 K threshold on IR geostationary data. To evaluate the impact of the geostationary IR data homogenization on high cold clouds, we compute the cold cloud fraction. The fraction is determined by applying a 235 K threshold on the initial  $BT_{GEO}$  before any corrections, on the spectrally adjusted and calibrated  $BT_{GEO}$  and finally on the VZA corrected IR data for the 2016 period and over the entire tropics. The computations are performed by using the selected configuration of the geostationary fleet and the map of cold cloud fraction provided on a  $1^\circ \times 1^\circ$  grid [Fig. 10(a)–(c)]. Before corrections, a local maximum of cold cloud fraction reaching 26% is seen in the Meteosat-7 area over the west coast of the Indo–China peninsula. However, the calibration correction allows to attenuate this fraction which falls to 22%. Also, note that this region is observed by Meteosat-7 with a VZA of  $47^\circ$ . After the limb-adjustment procedure, the value of cold cloud fraction for this specific region decreases to 17%. The maximum of cold cloud fraction is now located over the warm pool and is observed by the HIMAWARI-8 platform. One can also see that the local maximum of cold cloud fraction over the Tibetan plateau is strongly attenuated with all the corrections. Before applying the homogenization procedure, one can observe some steps of the conditional meridional average of cold cloud cover at the boundary of Meteosat-7 and HIMAWARI-8 and between HIMAWARI-8 and GOES-15, reaching 1.65% and 1.47%, respectively [Fig. 10(d)]. The combined corrections improve these issues and show a cold cloud cover exhibiting a smoother transition from one platform to another. Fig. 10(d) shows similar cold cloud covers for low VZA between a unique calibration/spectral correction and the combined calibration/spectral and VZA corrections, while one can observe a decrease in cold cloud cover for large VZA between the two corrections.

The extension of the current database beyond 2016 is under consideration. The configuration of the fleet, nevertheless, drastically changes in 2017 with the end of operation of Meteosat-7 and the arrival of MSG-1 in February on a shifted position, although not fully covering the Indian Ocean. Tests are needed to explore the sensitivity of the database to this new configuration. The use of INSAT-3D is also contemplated as a better way to bridge MSG-1 and HIMAWARI-8 data. GOES-R has become operational and the stream of GOES-16 replaces GOES-13 in December 2017. Similarly, GOES-17 is now operational as the new GOES west coverage replacing the GOES-15 platform from February 2019.

Up to the end of 2018, the Megha-Tropiques mission has been operated nominally granting the possibility of extending the present effort up to that time. While the present work relies on the ScaRaB instrument onboard Megha-Tropiques, it can easily be applied to alternative IR reference observations, from hyperspectral sounders, for instance. This article indicates that the final calibrated and limb-adjusted IR observations for  $BT < 240$  K can be homogeneous throughout the GEOring

with less than 1.5 K standard deviation, and that further future efforts should strive for such, or better, accuracy.

#### ACKNOWLEDGMENT

The authors would like to thank the ESPRI/IPSL team for providing computing and storage resources. They also thank the DWD as well as the French data center AERIS for their help in accessing the data (GEOring, ScaRaB). They also thank G. Urbani and C. Bovalo for their help in handling the geostationary satellite data archive. They further acknowledge M. Dejus, Project Manager at CNES, and his team for their help on the technical aspects of ScaRaB. The ScaRaB L2B is available in the ICARE data and service center with an *Anonymous File Transfer Protocol* ([ftp://ftp.icare.univ-lille1.fr/SPACEBORNE/SCARAB/MT1\\_L2B-FLUX-SCASL1A2\\_0.5deg.v2.01/](ftp://ftp.icare.univ-lille1.fr/SPACEBORNE/SCARAB/MT1_L2B-FLUX-SCASL1A2_0.5deg.v2.01/)). The calibration coefficients and the limb-adjustment coefficients are available at the following DOI: <https://doi.org/10.14768/20191125>.

#### REFERENCES

- R. A. Schiffer and W. B. Rossow, "The International Satellite Cloud Climatology Project (ISCCP): The first project of the World Climate Research Programme," *Bull. Amer. Meteorol. Soc.*, vol. 64, no. 7, pp. 779–784, Jul. 1983.
- M. L. Salby, H. H. Hendon, K. Woodberry, and K. Tanaka, "Analysis of global cloud imagery from multiple satellites," *Bull. Amer. Meteorol. Soc.*, vol. 72, no. 4, pp. 467–480, Apr. 1991.
- G. J. Huffman *et al.*, "The Global Precipitation Climatology Project (GPCP) combined precipitation dataset," *Bull. Amer. Meteorol. Soc.*, vol. 78, no. 1, pp. 5–20, 1997.
- K. R. Knapp *et al.*, "Globally Gridded Satellite observations for climate studies," *Bull. Amer. Meteorol. Soc.*, vol. 92, no. 7, pp. 893–907, Jul. 2011.
- R. A. Kohrs, M. A. Lazzara, J. O. Robaidek, D. A. Santek, and S. L. Knuth, "Global satellite composites—20 years of evolution," *Atmos. Res.*, vols. 135–136, pp. 8–34, Jan. 2014.
- P. Zhang, K. Holmlund, M. Goldberg, and J. Lafeuille, "The Global Space-based Inter-Calibration System (GSICS)," in *Proc. IEEE Int. Geosci. Remote Sens. Symp. (IGARSS)*, Jul. 2016, pp. 5522–5523.
- T. J. Hewison *et al.*, "GSICS inter-calibration of infrared channels of geostationary imagers using Metop/IASI," *IEEE Trans. Geosci. Remote Sens.*, vol. 51, no. 3, pp. 1160–1170, Mar. 2013.
- D. R. Doelling *et al.*, "Geostationary enhanced temporal interpolation for CERES flux products," *J. Atmos. Ocean. Technol.*, vol. 30, no. 6, pp. 1072–1090, Jun. 2013.
- T. J. Hewison and J. Muller, "Ice contamination of Meteosat/SEVIRI implied by intercalibration against Metop/IASI," *IEEE Trans. Geosci. Remote Sens.*, vol. 51, no. 3, pp. 1182–1186, Mar. 2013.
- B. Scarino, D. R. Doelling, C. Haney, K. Bedka, and P. Minnis, "Utilizing the precessing orbit of TRMM to produce hourly corrections of geostationary infrared imager data with the VIRS sensor," *Proc. SPIE*, vol. 10403, Aug. 2019, Art. no. 104030H.
- G. J. Robinson and K. I. Hodges, "Cloud archive user service user guide," Tech. Rep., 2005, p. 16.
- K. R. Knapp, "Gridded satellite B1 FCDR—Monthly means," Tech. Rep., 2016.
- J. E. Janowiak, R. J. Joyce, and Y. Yarosh, "A real-time global half-hourly pixel-resolution infrared dataset and its applications," *Bull. Amer. Meteorol. Soc.*, vol. 82, no. 2, pp. 205–217, Feb. 2001.
- Y. Desormeaux, W. B. Rossow, C. L. Brest, and G. G. Campbell, "Normalization and calibration of geostationary satellite radiances for the International Satellite Cloud Climatology Project," *J. Atmos. Ocean. Technol.*, vol. 10, no. 3, pp. 304–325, Jun. 1993.
- T. Fiolleau and R. Roca, "An algorithm for the detection and tracking of tropical mesoscale convective systems using infrared images from geostationary satellite," *IEEE Trans. Geosci. Remote Sens.*, vol. 51, no. 7, pp. 4302–4315, Jul. 2013.

[16] M. Schröder, M. König, and J. Schmetz, “Deep convection observed by the Spinning Enhanced Visible and Infrared Imager on board Meteosat 8: Spatial distribution and temporal evolution over Africa in summer and winter 2006,” *J. Geophys. Res.*, vol. 114, no. D5, pp. 1–14, 2009.

[17] B. E. Mapes and R. A. Houze, “Cloud clusters and superclusters over the oceanic warm pool,” *Monthly Weather Rev.*, vol. 121, no. 5, pp. 1398–1416, May 1993.

[18] R. Roca *et al.*, “The Megha-Tropiques mission: A review after three years in orbit,” *Frontiers Earth Sci.*, vol. 3, p. 17, May 2015.

[19] R. Kandel *et al.*, “The ScaRaB earth radiation budget dataset,” Natural Resour. Canada/ESS/Sci. Tech. Publishing Services, Tech. Rep., 1998.

[20] J.-P. Duvel *et al.*, “The ScaRaB-Resurs Earth radiation budget dataset and first results,” *Bull. Amer. Meteorol. Soc.*, vol. 82, no. 7, pp. 1397–1408, Jul. 2001.

[21] M. Viollier and P. Raberanto, “Radiometric and spectral characteristics of the ScaRaB-3 instrument on Megha-Tropiques: Comparisons with ERBE, CERES, and GERB,” *J. Atmos. Ocean. Technol.*, vol. 27, no. 3, pp. 428–442, Mar. 2010.

[22] A. Rosak, T. Tremas, N. Karouche, L. Gillot, and O. Simonella, “Radiometric and geometric Scarab-Megha-Tropiques ground calibration comparison with first in orbit calibration,” in *Proc. IEEE Int. Geosci. Remote Sens. Symp.*, Jul. 2012, pp. 4746–4749.

[23] N. Karouche, C. Goldstein, A. Rosak, C. Malassingne, and G. Raju, “MEGHA-TROPIQUES satellite mission: In flight performances results,” in *Proc. IEEE Int. Geosci. Remote Sens. Symp.*, Jul. 2012, pp. 4684–4687.

[24] T. L. Trémas, N. Karouche, A. Rosak, A. Meygret, O. Aznay, and E. Hillairet, “ScaRaB: First results of the scanner for radiative budget on board the Indo-French satellite Megha-Tropiques,” *Proc. SPIE*, vol. 8510, Oct. 2012, Art. no. 851002.

[25] R. Roca *et al.*, “Le bilan scientifique de la mission Megha-Tropiques après 8 ans dans l’espace,” *La Météorologie*, no. 107, p. 36, 2019.

[26] J. P. Duvel and P. Raberanto, “A geophysical cross-calibration approach for broadband channels: Application to the ScaRaB experiment,” *J. Atmos. Ocean. Technol.*, vol. 17, no. 12, pp. 1609–1617, Dec. 2000.

[27] D. R. Doelling, D. Morstad, B. R. Scarino, R. Bhatt, and A. Gopalan, “The characterization of deep convective clouds as an invariant calibration target and as a visible calibration technique,” *IEEE Trans. Geosci. Remote Sens.*, vol. 51, no. 3, pp. 1147–1159, Mar. 2013.

[28] G. L. Smith, Z. P. Szewczyk, K. J. Priestley, and R. Roca, “Method of comparing CERES and ScaRaB 3 measurements,” in *Proc. Sensors, Syst., Next-Gener. Satellites XVI SPIE*, 2012, pp. 7193–7196.

[29] T. L. Trémas, O. Aznay, and O. Chomette, “ScaRaB and CERES-Terra: Results of the inter-comparison campaigns,” *Proc. SPIE*, vol. 9973, Sep. 2016, Art. no. 99730B.

[30] N. Gif, O. Chomette, and P. Raberanto, “Co-location algorithms geophysical data projection using pixel point spread function,” Megha-Tropiques Tech. Memo. 2, 2011.

[31] M. Capderou, “Sampling. Comparison with other Meteorological Satellites,” Megha-Tropiques Tech. Memo. 1, 2009.

[32] C. L. Brest, W. B. Rossow, and M. D. Roiter, “Update of radiance calibrations for ISCCP,” *J. Atmos. Ocean. Technol.*, vol. 14, no. 5, pp. 1091–1109, Oct. 1997.

[33] K. R. Knapp, “Calibration assessment of ISCCP geostationary infrared observations using HIRS,” *J. Atmos. Ocean. Technol.*, vol. 25, no. 2, pp. 183–195, Feb. 2008.

[34] M. König, J. Schmetz, and S. Tjemkes, “Satellite intercalibration of IR window radiance observations,” *Adv. Space Res.*, vol. 23, no. 8, pp. 1341–1348, Jan. 1999.

[35] R. Joyce, J. Janowiak, and G. Huffman, “Latitudinally and seasonally dependent zenith-angle corrections for geostationary satellite IR brightness temperatures,” *J. Appl. Meteorol.*, vol. 40, no. 4, pp. 689–703, Apr. 2001.

[36] T. H. von der Haar and S. Q. Kidder, *Satellite Meteorology—An Introduction*. New York, NY, USA: Academic, 1995.

[37] M. D. Goldberg, D. S. Crosby, and L. Zhou, “The limb adjustment of AMSU—A observations: Methodology and validation,” *J. Appl. Meteorol.*, vol. 40, no. 1, pp. 70–83, Jan. 2001.

[38] Q. Liu and F. Weng, “Uses of NOAA-16 and -18 satellite measurements for verifying the limb-correction algorithm,” *J. Appl. Meteorol. Climatol.*, vol. 46, no. 4, pp. 544–548, Apr. 2007.

[39] P. Minnis, “Viewing zenith angle dependence of cloudiness determined from coincident GOES east and GOES west data,” *J. Geophys. Res.*, vol. 94, no. D2, pp. 2303–2320, 1989.

[40] N. J. Elmer, E. Berndt, and G. J. Jedlovec, “Limb correction of MODIS and VIIRS infrared channels for the improved interpretation of RGB composites,” *J. Atmos. Ocean. Technol.*, vol. 33, no. 5, pp. 1073–1087, May 2016.

[41] K. I. Hodges, D. W. Chappell, G. J. Robinson, and G. Yang, “An improved algorithm for generating global window brightness temperatures from multiple satellite infrared imagery,” *J. Atmos. Ocean. Technol.*, vol. 17, no. 10, pp. 1296–1312, Oct. 2000.



**Thomas Fiolleau** received the Ph.D. degree from Ecole Polytechnique, Paris, France, in 2010 with a thesis on the use of satellite observation to study mesoscale convective systems in the framework of the Megha-Tropiques Indo-French Satellite Mission.

He was an Associate Engineer with the Laboratoire de Météorologie Dynamique (LMD), Paris, for two years. He worked as a United Nations Educational, Scientific and Cultural Organization (UNESCO) Consultant with the Centro Nacional de Monitoramento e Alertas de Desastres Naturais (CEMADEN), Brazil, a Brazilian operational center, where he worked on the development of operational algorithms to forecast convective systems. After two years at CNRM (joint laboratory between CNRS and Météo-France), he joined the CNRS in 2016 as a Research Engineer with the Laboratoire d’Etudes en Géographie et Océanographie Spatiales, Toulouse, France. His areas of specialization are remote sensing, image processing, tropical climate and meteorology, and his researches interests are focused on the development of cloud tracking algorithms from geostationary satellites and the study of the life cycle of tropical mesoscale convective systems by using satellite observations.



**Rémy Roca** received the M.S. degree in fundamental physics, with major in remote sensing, and the Ph.D. degree in 2000 from Université Paris, Paris, France, with a thesis on the use of satellite observations to evaluate climate models.

He was with the Scripps Institution of Oceanography, University of California, San Diego, CA, USA, for almost two years where he got familiar with image processing and cloud detection and tracking algorithms from geostationary satellites. From 2001 to 2012, he was with the Laboratoire de Météorologie Dynamique, Institut Pierre et Simon Laplace, Paris, where he was a CNRS Researcher. He was appointed a Mission Scientist of the Megha-Tropiques Indo-French Satellite Mission and took over the PIship of the mission in 2007. He is a Senior CNRS Researcher with the Laboratoire d’Etudes en Géographie et Océanographie Spatiales, Toulouse, France. His broad interests are focused on the study of the water cycle in the tropics and the use of satellite observations to investigate the tropical variability. He has more than 15 years of experience in the field of tropical climate, meteorology, and remote sensing.

Dr. Roca was the Chairman of the International Precipitation Group in 2014 and 2015, and since 2016, he has been co-leading the GEWEX/WCRP Data Analysis Panel.



**Sophie Cloché** received the M.S. degree in fundamental physics, with a specialization in remote sensing, and the Ph.D. degree in 1996 with a thesis on the use of satellite observations (POLDER) for cloud and water vapor detection from Université Paris, Paris, France.

From 1996 to 1998, she was a Post-Doctoral Position with the Laboratoire de Météorologie Dynamique (LMD/CNRS), Paris, working on narrow to broadband conversion to estimate the radiative fluxes. From 1998 to 2001, she was as a Research Engineer, on database management for the INDOEX program, LMD. In 2001, she obtained a fix position with the CNRS, Institut Pierre-Simon Laplace (IPSL), Paris, as Research Engineer, and also involved in database management for different national and international projects (AMMA, Hymex, GEWEX-Cloud Assessment for example). She is the Co-ordinator of the scientific ground segment for the Megha-Tropiques mission and involved in the CM SAF from Eumetsat for the development of a global precipitation product. She also coordinates space activities at IPSL and she is responsible of the database management of observations at IPSL.

AQ:9

AQ:10

AQ:11

856  
857  
858  
859  
860  
861  
862  
863  
864  
865  
866  
867  
868  
869  
870  
871  
872  
873  
874  
875  
876  
877  
878  
879  
880  
881  
882  
883  
884  
885  
886  
887  
888  
889  
890  
891  
892  
893  
894  
895  
896  
897  
898  
899  
900  
901  
902  
903  
904  
905  
906  
907  
908  
909  
910  
911  
912  
913  
914  
915  
916  
917  
918  
919  
920  
921  
922  
923  
924  
925  
926  
927

AQ:12

AQ:13

928  
929  
930  
931  
932  
933  
AQ:14 934  
935  
936  
937  
938  
939  
940  
941  
942  
943  
944



**Dominique Bouniol** received the Ph.D. degree from the University of Paris, Paris, France, in 2000, with a thesis on process-oriented use of observational data sets for understanding mesoscale storm deepening.

After 18 months in the Radar Meteorology Group, University of Reading, Reading, England, she joined the CNRS as a Researcher in 2002, first in CETP where she was involved in the implementation and exploitation of ground-based cloud radar in the framework of the Cloudnet project. She led the deployment of the airborne version of the cloud radar

within the AMMA experiment in Niger and Senegal, in 2006. While she was with CNRS, she joined the CNRM (joint laboratory between CNRS and Météo-France), in 2006, where her research focuses on physical processes involved in the tropical mesoscale convective system life cycle and more generally on tropical cloud processes using both observations and modeling tools.



**Patrick Raberanto** received the Ph.D. degree in astronomy and space technology from Paul Sabatier University, Toulouse, France, in 1984.

In 1990, he joined the Laboratoire de Météorologie Dynamique (LMD), Ecole Polytechnique, Paris, as a CNRS Research Engineer and was implied in the ScaRaB project. In the framework of the Megha-Tropiques mission, he was in charge of the ScaRaB calibration, validation, and the development of the ScaRaB level-2 products. His research interests include radiometric calibration and radiative budget observation.

945  
946  
947  
948  
949  
950  
951  
952  
953  
954  
955  
956

IEEE Proof